NASA TECHNICAL MEMORANDUM

NASA TM X-3179

NASA TM X-3179

METHOD OF REPRESENTATION OF ACOUSTIC SPECTRA AND REFLECTION CORRECTIONS APPLIED TO EXTERNALLY BLOWN FLAP NOISE

Jeffrey H. Miles

Lewis Research Center

Cleveland, Ohio 44135

NATIONAL AERONAUTICS AND SPACE ADMINISTRATION • WASHINGTON, D. C. • FEBRUARY 1975

1. Report No.	2. Government Accession No.	3. Recipient's Catalog No.
NASA TM X-3179		

4. Title and Subtitle	5. Report Date
METHOD OF REPRESENTATION OF ACOUSTIC SPECTRA AND REFLECTION CORRECTIONS APPLIED TO EXTERNALLY BLOWN FLAP NOISE	February 1975
	6. Performing Organization Code
7. Author(s)	8. Performing Organization Report No.
Jeffrey H. Miles	E-8043
	10. Work Unit No.
9. Performing Organization Name and Address	501-24
Lewis Research Center National Aeronautics and Space Administration Cleveland, Ohio 44135	11. Contract or Grant No.
	13. Type of Report and Period Covered
12. Sponsoring Agency Name and Address	Technical Memorandum
National Aeronautics and Space Administration Washington, D.C. 20546	14. Sponsoring Agency Code

15. Supplementary Notes

16. Abstract

A computer method for obtaining a rational function representation of an acoustic spectrum and for correcting reflection effects is introduced. The functional representation provides a means of compact storage of data and the nucleus of the data analysis method. The method is applied to noise from a full-scale externally blown flap system with a quiet 6:1 bypass ratio turbofan engine and a three-flap wing section designed to simulate the take-off condition of a conceptual STOL aircraft.

17. Key Words (Suggested by Author(s))		18. Distribution Statement
Aircraft noise	Jet aircraft noise	Unclassified - unlimited
Noise (sound)	Acoustics	STAR category 45 (rev.)
Noise spectra		

19. Security Classif. (of this report)	20. Security Classif. (of this page)	21. No. of Pages	22. Price*
Unclassified	Unclassified	68	$3.75

* For sale by the National Technical Information Service, Springfield, Virginia 22151

METHOD OF REPRESENTATION OF ACOUSTIC SPECTRA AND REFLECTION CORRECTIONS APPLIED TO EXTERNALLY BLOWN FLAP NOISE

by Jeffrey H. Miles

Lewis Research Center

SUMMARY

A computer method for obtaining a rational function representation of an acoustic spectrum and for correcting reflection effects is introduced. The reflection effects were estimated from one-third-octave sound pressure level (SPL) data. The reflection and atmospheric attenuation effects were taken into account at the time the power spectral density function needed to represent the measured SPL was selected. The procedure is based on minimizing the square of the error between the measured SPL and the calculated SPL.

The most important results obtained were that (1) a rational polynomial with a first-order numerator and a third-order denominator was a satisfactorily expressed Strouhal normalized mean-square pressure spectral density level and (2) the N independent source model of P. Thomas was satisfactory in calculating the reflection effects when this model was extended by the use of a reflected-ray transfer function. The computer procedure was applied to noise from a full-scale externally blown-flap system having a three-flap wing section with a quiet 6:1 bypass ratio turbofan engine having a coannular nozzle. The three-flap wing section simulates the take-off condition of a conceptual STOL aircraft.

INTRODUCTION

Short takeoff and landing (STOL) aircraft may become an important means of transportation in urban areas. But, strong adverse public reaction to aircraft noise means that future STOL aircraft may be required to meet stringent noise level regulations. Thus, noise will be one of the primary factors in the selection of a STOL propulsion-lift system. One candidate source of propulsive-lift is the externally blown-flap (EBF) system.

Each EBF STOL concept introduces noise sources not present in conventional take-off and landing (CTOL) airplanes. These EBF STOL propulsive-lift concepts are being investigated by both scale-model and full-scale engine tests. Concurrently, theoretical and experimental studies are being conducted on various noise source mechanisms, and empirical prediction methods are being devised.

In a recent study conducted at Lewis (ref. 1), a rational function representation of flap noise spectra was shown to be useful (1) as an empirical equation to fit EBF STOL spectral data, (2) as a function that can be related to certain noise-source mechanisms, and (3) as part of a computer method for making corrections to acoustic reflections in static test data. An objective of this report is to provide the details in the development of the equations described in reference 1.

In spite of many advances in the understanding of noise sources, procedures for calculating noise from EBF STOL airplanes starting with basic aeroacoustic mechanisms are not currently available. Hence present design studies depend on model and full-scale tests and on empirical relations determined from these tests.

For design studies a most important aspect of the measured noise is the one-third-octave sound-pressure level spectrum designated in this report by SPL. It is used to compute the perceived noise level (PNL) and the effective perceived noise level (EPNL), which are the criteria presently used to judge the effect of aircraft noise on the community.

The empirical rational function discussed in reference 1 may be used to represent broad-band SPL spectrum data. With the representation described, sound spectra can be stored in a computer in a compact form and thus facilitate comparison of large amounts of data from different experiments. The representation can also be used to extrapolate data to untested conditions and is useful in making estimates of PNL, EPNL, and footprint calculations.

Another objective of this report is to provide an example of the application of this empirical rational function representation to a set of data. As an example, the procedure is applied to data from a full-scale externally blown-flap (EBF) system with a three-flap wing section. The EBF propulsion system is operated to simulate the takeoff condition. The wing section is positioned to simulate the takeoff condition of a conceptual STOL airplane (ref. 2). The data are from an acoustic program conducted under the direction of Lewis using a quieted 6:1 bypass ratio turbofan engine having a coannular nozzle (refs. 3 and 4). Reflection effects evident in this research program make it a good example to demonstrate the use of the procedure.

ANALYSIS

APPROACH

The approach taken to represent the measured flap noise spectra is based on a model that assumes the measured one-third-octave band SPL spectrum can be represented as the sum of a lossless spectrum SPL^+, a ground reflectance $|T|^2$, and an atmospheric attenuation level A_T. Thus, $SPL = SPL^+ + 10 \log_{10}|T|^2 + A_T$, dB referenced to 2×10^{-5} Pa[1] (2×10^{-4} μ bar). The same approach was used in reference 1 where a condensed description appears.

The approach taken to represent the lossless spectra will be discussed first. Since the development is long, references will be made to appendixes for the details. Next, the equations necessary to relate the lossless SPL to the SPL with ground reflection effects will be discussed. Finally these results will be used in presenting the complete model.

LOSSLESS SPECTRAL DENSITY

A semiempirical method of representing SPL spectra was briefly described in reference 1 and is presented herein in greater detail. Other procedures for describing externally blown-flap SPL spectra are described in references 5 and 6. But, these methods are not as universally applicable as the method described.

Spectral Density Function

The approach taken to represent the lossless flap noise spectra is based on finding a function of Strouhal number $\varphi(\Omega)$ such that the one-third-octave lossless sound pressure level (SPL^+) can be fitted by

$$SPL^+(l) = 10 \log \left\{ (10^{OASPL/10}) \left[\Delta f_c(l) \frac{D_e}{V_e} \right] \varphi(\Omega) \right\} \tag{1}$$

where

$$OASPL = 10 \log \sum_{l} 10^{SPL(l)/10} \tag{2}$$

[1] 1 Pascal (symbol Pa) equals 1 N/m^2.

and where D_e is an effective diameter (ref. 7), V_e is an effective velocity (ref. 7), $\Delta f_c(l)$ is the band width of the one-third-octave band having a center frequency f_c, and l is the l^{th} one-third-octave frequency band. (All symbols are defined in appendix A.) Specifically,

$$\Omega = j2\pi \left(f_c \frac{D_e}{V_e} \right) = j2\pi \, St \tag{3}$$

where

$$j = \sqrt{-1}$$

and St is the Strouhal number.

The semiempirical method to be discussed uses a certain function $\varphi(\Omega)$ to represent the lossless flap noise spectra. The function was developed to represent spectra having only a single peak. Thus, for example, the function would be applicable to represent single and coannular nozzle jet noise data and EBF noise produced by a single or a coannular jet blowing on a flap. Other requirements on the function $\varphi(\Omega)$ follow:

(1) The function should be tailored for applicability to large Strouhal numbers. Curve fits that are accurate at large Strouhal numbers are necessary, since EBF engines are likely to have large effective diameters and low velocities.

(2) It should be consistent with theoretical considerations.

(3) It should depend on as few mathematical coefficients and operations as possible since this will reduce computer calculation time.

(4) It should be applicable to a wide range of system configurations (e.g., single or coannular nozzles, over-the-wing and under-the-wing).

From equation (1) $10 \log_{10}[\varphi(\Omega)]$ becomes

$$10 \log_{10} \left[\varphi(\Omega) \right] \Big|_{\Omega = j2\pi f_c(l)} = SPL(l) - OASPL - 10 \log_{10} \left[\Delta f_c(l) \frac{D_e}{V_e} \right] \tag{4a}$$

The quantity represented by equation (4a) is the Strouhal normalized mean-square pressure spectral density level. In this report, expression (4a) will be referred to as the PSD^+ function of Strouhal number. Specifically, PSD^+ is calculated from or represents SPL data free of atmospheric absorption and reflection effects (lossless data). Thus

$$PSD^+ = 10 \log_{10} \left[\varphi(\Omega) \right] \tag{4b}$$

The selected relation for lossless flap noise spectra given by equations (1) and (4b) is based on EBF experimental evidence, acoustic noise theory, and spectral analysis theory. It has been shown that spectral data taken over a range of exhaust velocities for numerous over-the-wing and under-the-wing EBF configurations correlate when plotted in terms of the PSD^+ function (refs. 7 to 9). Furthermore, the functional form of equation (4a) was used to correlate noise from jets (refs. 10 to 12). It was also used to correlate total sound power spectrum data taken over a range of exhaust velocities of various EBF model configurations (refs. 13 and 14).

Theory and Experiments Related to Externally Blown Flap Noise

The semiempirical method of representing the EBF sound spectral density was related in reference 1 to certain theoretical and experimental work on noise source mechanisms believed to be related to EBF noise. Extensive work has been done in studying many EBF noise source mechanisms (refs. 5, 6, and 15 to 26). Some of these theoretical studies try to relate the turbulence spectral density to the sound spectral density. These theoretical studies require detailed information about the nature of the turbulence spectral density beyond that contained in reference 27 to make accurate predictions.

An important noise source for EBF systems is scrubbing noise generated in the turbulent boundary layer by the jet mixing region and convected along the wing or flap. Attempts have been made to relate the turbulence spectral density associated with scrubbing to the noise produced (refs. 24 and 26). The necessary turbulence spectral density data used in reference 26 was obtained from references 28 to 30.

The semiempirical method of representing the EBF sound pressure spectral density (ref. 1) was developed so that it could be related to a scrubbing noise source as described in references 24 and 26. The approach used was based on the theory of spectral analysis and realizable linear filters as described in references 31 to 36. Certain procedures were adopted from modern control theory (ref. 37). The basic definition of one-third-octave spectra is that specified in reference 38.

Development of Spectral Density Function

The one-third-octave sound pressure level spectrum approximates the mean-square pressure spectral density of a real stationary random process. The same information that is present in the spectral density is present in the covariance function of a stationary real random process. The equations expressing these relations are stated in appen-

dix B. These equations are based on spectral analysis theory. To represent a mean-square pressure spectrum of a real random process these functions must be nonnegative, integrable, and an even function of frequency.

The spectral density of many real random processes can be represented by a certain general function form. This form, called a rational function, is described in appendix C. By analogy it will be assumed that $\varphi(\Omega)$ can be expressed as a function having the same basic form (see appendix C).

A particular realization of this general form is selected. This realization involves the use of a function formulated from the Fourier transform of a "damped cosine oscillation." This function is discussed in appendix D. The resulting formula for $\varphi(\Omega)$ is denoted as the basic spectral density function $\varphi_{real}(\Omega)$. This function can be written as the sum of basic Strouhal response curves (appendix E).

The basic spectral density was used in reference 1 to fit PSD^+ data. A good fit was achieved with data from an under-the-wing EBF configuration and an over-the-wing configuration with attached flap flow (powered lift) and with unattached flap flow (conventional lift). Reference 1 also shows the basic spectral density function to be related to the theory of scrubbing noise as described in references 24 and 26.

Although the basic spectral density function satisfies some of the requirements, a function that uses less computer time can be formulated from this expression. (See appendix F.) The new function is empirical and since it is not an even function of frequency it is not a spectral density. However, since it has the other properties of the basic spectral density, the new functional form of $\varphi(\Omega)$, denoted as the simplified spectral density function $\varphi_{cal}(\Omega)$ was used to curve fit the data discussed herein. This function can be written as the sum of simplified Strouhal response curves (appendix F). Reference 1 shows that this function was also satisfactory in fitting many EBF sets of data.

The simplified lossless spectral density function is

$$\varphi_{cal}(\Omega) = \left| \frac{a_o \prod_{i=1}^{M_a} (\Omega - a_i)}{\prod_{k=1}^{N_b} (\Omega - b_k)} \right|^2 = \left| \frac{a(\Omega)}{b(\Omega)} \right|^2 \qquad \text{(F1)}$$

where a_o is a normalization parameter determined by the requirement that the integral from zero to infinity of the spectral density is unity, a_i: $i = 1, \ldots, M_a$ and b_k: $k = 1, \ldots, N_b$ are complex parameters with negative real parts and positive imaginary parts, $a(\Omega)$ is a polynomial equation of order M_a, and $b(\Omega)$ is a polynomial equation of order N_b.

Thus, the approach taken to represent lossless flap noise spectra is based on the equation obtained by substituting equation (F1) into equation (1). The resulting equation can be fitted to one-third-octave lossless SPL spectra with the proper selection of the OASPL, a_i, and b_k parameters. After developing the reflection correction, the calculation method used to select these parameters will be discussed.

REFLECTION CORRECTION

It has been assumed that the measured spectrum can, in part, be represented as the sum of a lossless spectrum and a ground reflectance. The function used to represent the lossless spectrum was discussed in the last section. In this section the equation used to represent the reflectance will be derived.

The effect of interference due to reflections is strongly dependent on test facility geometry. The analysis of these effects is based on the EBF test facility geometry of reference 2. Figure 1(a) shows the source-microphone geometry with respect to the ground plane. The wing flap system is shown in figure 1(b), and the microphone array in figure 1(c). The basic concepts used in the simple mathematical model that will be described for this setup are presented next to reveal some of the complications hidden by the approach used.

The mathematical model deals with the reflection problem even though a good physical description of it is lacking because the data were measured in one-third-octave bands and thus provide only limited information representing an average over each band. Only one of several possible interpretations of the mathematical model will be considered in the analysis. The working hypothesis will be that the noise can be treated as if it were from a vertical (spanwise) arrangement of independent sources of equal strength at the trailing edge of the third flap (fig. 1(a)). The choice of this physical model to represent the measured effects does not indicate that this model is the best physical description of the true noise source. The EBF data in references 8, 13, and 14 indicate that leading-edge noise, trailing edge noise, flap surface noise, and redirection of jet noise are all possible contributors. Opinions on the dominant noise source differ.

The effect of reflections are dealt with using an acoustic ray theory. But the approach used differs in that the reflected ray is assumed to be related to the direct ray by a convolution integral of the reflecting surface's impulse response with the direct pressure wave. The Laplace transform of this impulse response is called the reflected-ray transfer function.

Model and Assumptions

The interference due to reflections causes cancellations and reinforcements to occur in certain one-third-octave SPL bands. In the example considered, the distance from the source to the microphone is large compared with the source or microphone heights above the ground (fig. 1(c)). Thus, to a large extent, changes in the longitudinal location of the vertical array of sources does not shift the one-third-octave band in which a cancellation or reinforcement occurs. Hence, it is assumed sufficient to use, for these calculations, as the distance between source array and microphone the radius measured from the center of the jet nozzle exit to the microphone.

To simplify the model the following assumptions are made: (1) The reflected-ray transfer function is the same for each of the equal independent sources in the vertical array. (2) At different microphone angles the reflected-ray transfer function changes. For a model of N independent sources of equal strength at the trailing edge of the third flap, this could be interpreted as being due to the reflected rays from the trailing edge of the third flap traveling more than one path to get to a particular microphone. The model having N independent sources of equal strength at the trailing edge of the third flap will be called the multiple reflection model. Because of the large size of the wing flap system (fig. 1(b)), the wing and flaps are important factors (along with the ground) in producing the observed reflection effects.

The vertical displacement distances of the selected sources from the jet axis for each of the sources is determined by the test configuration (fig. 1). This distance yields the one-third-octave range over which the calculated cancellations and reinforcements extend. As previously mentioned, the multiple reflection model is not sensitive to changes in path length changes due to reflections from the wing-flap system. (It is possible that the variations of the reflected-ray transfer function are actually due to variations in the source strength in the vertical source plane or to the interaction of the various possible noise sources, producing different reflection effects at different angles from the flap.)

A derivation of the reflectance that can be used to represent the effect of ground to wing-flap reflections on the sound produced by the wing-flap system interacting with the coannular jet is given next. The model assumes that the source is distributed over a region and approximates this by considering the rays from N independent point sources. This assumption was used by P. Thomas to study acoustic interference of the noise produced by a single jet due to reflections from a plane (ref. 39). An alternative treatment for a distributed source using the wave equation is given in reference 40. The ground reflection effect on a single point source has been treated in references 41 to 44.

Derivation of Equations

The noise sources, flap, and microphone geometry with respect to the ground plane are shown in figure 1(a). Each of the N independent sources is assumed to produce a direct ray that travels a distance s_1. All the sources are assumed to be at a fixed distance r from all the microphones. For the n^{th} source at a height $h_s(n)$,

$$s_1(n) = \left\{r^2 + \left[h_s(n) - h_o\right]\right\}^{1/2} \tag{5}$$

where h_o is the microphone height. Each source, as previously mentioned, is also hypothesized to produce multiple reflected rays that travel distances s_2'. The reflections the rays undergo vary with microphone position because different multiple reflections are undergone by the reflected rays that reach each microphone.

Calculations must only be accurate enough to locate cancellations and reinforcements in the proper one-third-octave band. Thus the assumption can be made that the path length difference between the direct-ray path and reflected-ray path from the source to the wing flap to the ground to the microphone is nearly equal to the path length difference between the direct-ray path and reflected-ray path from the source to the ground to the microphone. This reflected-ray path distance is, for the n^{th} source

$$s_2(n) = \left\{r^2 + \left[h_s(n) + h_o\right]^2\right\}^{1/2} \tag{6}$$

The sound reaching the microphone is assumed to consist of the sound that travels the direct path and the sound that travels the reflected path. Since the reflected path is longer than the direct path, the reflected sound reaches the microphone after a time delay τ where

$$\tau = \frac{(s_2 - s_1)}{c_o} \tag{7}$$

(where c_o is the velocity of sound) relative to the direct sound that left at the same time. Thus if the direct wave reaching the microphone was emitted at a time t, the reflected wave reaching the microphone at the same time is due to one emitted at an earlier time $t - \tau$.

The effect of the multiple reflections on the reflected wave is related to the direct wave as follows: Let p(t) be the direct normalized pressure wave incident on the micro-

phone. Then for the n^{th} source the reflected wave from the wing-flap and ground surfaces can be related to the direct wave, with the time delay τ_n and the distance ratio $1/z_n$ accounted for, by the convolution integral of the reflecting surface's impulse response with the direct pressure wave. Thus

$$\frac{1}{z_n} p_n'(t - \tau_n) = \frac{1}{z_n} \int_0^\infty g(\tau - \tau_n) p(t - \tau)\, d\tau$$

where

$$z_n = \frac{s_2(n')}{s_1(n)}$$

Removing the inverse distance and the time-delay effects results in a definition of the effect of the reflecting surfaces:

$$p_n'(t) = \int_0^\infty g(\tau) p(t - \tau)\, d\tau \tag{8}$$

where $g(\tau)$ is the impulse of the reflecting surfaces. The reflected-ray transfer function $G(s)$ is defined as the Laplace transform of the impulse response g:

$$e^{-\tau_n s} G(s) = \int_0^\infty g(t - \tau_n) e^{-\tau s}\, d\tau$$

or

$$G(s) = \int_0^\infty g(\tau) e^{-\tau s}\, d\tau \tag{9}$$

This complex reflected-ray transfer function can also be written in terms of its phase δ and amplitude Q as

$$G(s) = Q(s) e^{j\delta(s)} \tag{10}$$

The observed normalized pressure at a distance r will be

$$P(t, \tau_n) = \sum_{n=1}^{N} p_n(t) + \sum_{n'=1}^{N} \frac{1}{z_{n'n}} p'_{n'}(t - \tau_{n'n}) \tag{11}$$

where

$$\tau_{n'n} = \delta_{n'n} \frac{\left[s_2(n') - s_1(n)\right]}{c_o} \tag{12}$$

$$z_{n'n} = \delta_{n'n} \frac{s_2(n')}{s_1(n)} \tag{13}$$

The variation of the heights of the sources, relative to the radial distance is assumed small; thus the value of $z_{n'n}$ will be replaced by a mean value z. Also $\tau_{n'n}$ will be denoted by τ_n.

The resultant normalized mean-square pressure spectrum density at the microphone will be found by a two-step procedure. First the autocorrelation of the signal will be found. Then the Laplace transform of the autocorrelation will be taken. This two-step procedure must be used to obtain the frequency response, because the noise is assumed to be produced by a stationary independent random process.

The autocorrelation of the relative pressure signal received by the microphone is

$$R_{tot}(\xi) = E\left\{P(t, \tau_n), P(t + \xi, \tau_n)\right\} \tag{14}$$

where $E\{\ \}$ denotes taking an ensemble average (see appendix B). Substituting equation (11) into equation (14) yields

$$R_{tot}(\xi) = E\left\{\left[\sum_{n=1}^{N} p_n(t) + \frac{1}{z} \sum_{n'=1}^{N} p'_{n'}(t - \tau_n)\right]\left[\sum_{n=1}^{N} p_n(t + \xi) + \frac{1}{z} \sum_{n'=1}^{N} p'_{n'}(t - \tau_n + \xi)\right]\right\} \tag{15}$$

Since each source is assumed to be independent, the calculation can proceed using one source, and the result can be summed to obtain the effect of N sources. For the n^{th} individual source

$$R_{tot,n}(\xi) = E\left\{\left[p_n(t) + \frac{1}{z}\,p_n'(t - \tau_n)\right]\left[p_n(t + \xi) + \frac{1}{z}\,p_n'(t - \tau_n + \xi)\right]\right\} \tag{16}$$

This equation when expanded becomes

$$R_{tot,n}(\xi) = E\left\{p_n(t)p_n(t + \xi)\right\} + \frac{1}{z}\,E\left\{p_n(t)p_n'(t - \tau_n + \xi)\right\}$$

$$+ \frac{1}{z}\,E\left\{p_n'(t - \tau_n)p_n(t + \xi)\right\} + \frac{1}{z^2}\,E\left\{p_n'(t - \tau_n)p_n'(t - \tau_n + \xi)\right\}$$

$$= R_n(\xi) + \frac{1}{z^2}\,R_n'(\xi) + \frac{1}{z}\left[E\left\{p_n(t)p_n'(t - \tau_n + \xi)\right\} + E\left\{p_n'(t - \tau_n)p_n(t + \xi)\right\}\right] \tag{17}$$

The Laplace transform of the autocorrelation $R_{tot,n}(\xi)$ is the spectral density of the source $H_n(s)$ with reflection effects included:

$$H_n(s) = \int_0^\infty R_{tot,n}(\xi)e^{-\xi s}\,d\xi \tag{18}$$

Substituting equation (8) and (17) into equation (18), we obtain

$$H_n(s) = \int_0^\infty R_{tot,n}(\xi)e^{-\xi s}\,d\xi$$

$$+ \frac{1}{z^2}\int_0^\infty e^{-\xi s}E\left\{\int_0^\infty g(\tau_1)p_n(t - \tau_1)\,d\tau_1 \int_0^\infty g(\tau_2)p_n(t + \xi - \tau_2)\,d\tau_2\right\}d\xi$$

$$+ \frac{1}{z}\int_0^\infty e^{-\xi s}E\left\{p_n(t)\int_0^\infty g(\tau)p_n(t - \tau_n + \xi - \tau)\,d\tau\right\}d\xi$$

$$+ \frac{1}{z}\int_0^\infty e^{-\xi s}E\left\{\int_0^\infty g(\tau)p_n(t - \tau)\,d\tau\, p_n(t + \xi + \tau_n)\right\}d\xi \tag{19}$$

The first term on the right of equation (19) is the source spectrum of the n^{th} source

$$S_n(s) = \int_0^\infty R_n(\xi)e^{-\xi s}\, d\xi \tag{20}$$

The second term on the right hand side of equation (19) is evaluated next. Using equation (9) and (20)

$$\int_0^\infty e^{-\xi s} E\left\{\int_0^\infty g(\tau_1)p_n(t - \tau_1)\, d\tau_1 \int_0^\infty g(\tau_2)p_n(t - \tau_2 + \xi)\, d\tau_2\right\} d\xi$$

$$= \int_0^\infty e^{-\xi s} \int_0^\infty g(\tau_1)\, d\tau_1 \int_0^\infty g(\tau_2)R_n(\xi - \tau_2 + \tau_1)\, d\tau_2\, d\xi$$

$$= \int_0^\infty g(\tau_1)e^{-\tau_1 s}\, d\tau_1 \int_0^\infty g(\tau_2)e^{\tau_2 s}\, d\tau_2 \int_0^\infty e^{-\sigma s}R_n(\sigma)\, d\sigma$$

$$= G(s)G^*(s)S_n(s) \tag{21}$$

The third and fourth terms on the right hand side of equation (19) are also evaluated using equations (9) and (20). Thus

$$\int_0^\infty e^{-\xi s} E\left\{p_n(t) \int_0^\infty g(\tau)p_n(t - \tau_n + \xi - \tau)\, d\tau\right\} d\xi$$

$$= \int_0^\infty e^{-\xi s} \int_0^\infty g(\tau)\, d\tau\, R_n(\xi - \tau_n - \tau)\, d\xi$$

$$= e^{\tau_n s} \int_0^\infty e^{-\sigma s}R_n(\sigma)\, d\sigma \int_0^\infty e^{\tau s}g(\tau)\, d\tau$$

$$= e^{\tau_n s} G^*(s)S_n(s) \tag{22}$$

and

$$\int_0^\infty e^{-\xi s} E\left\{ p_n(t + \xi + \tau_n) \int_0^\infty g(\tau) p_n(t - \tau)\, d\tau \right\} d\xi$$

$$= \int_0^\infty e^{-\xi s} \int_0^\infty g(\tau)\, d\tau\, R_n(\xi + \tau_n + \tau)\, d\xi$$

$$= e^{-\tau_n s} \int_0^\infty e^{-\sigma s} R_n(\sigma)\, d\sigma \int_0^\infty e^{-\tau s} g(\tau)\, d\tau$$

$$= e^{-\tau_n s} G(s) S_n(s) \tag{23}$$

Substituting equations (20) to (23) into equation (19), the spectrum due to a single source with reflections included is

$$H_n(s) = S_n(s) + \frac{1}{z^2} G(s) G^*(s) S_n(s) + \frac{1}{z} \left\{ G(s) e^{-\tau_n s} + \left[G(s) e^{-\tau_n s} \right]^* \right\} S_n(s) \tag{24}$$

The normalized mean-square pressure spectrum density due to N independent sources is then

$$H(s) = \sum_{n=1}^{N} H_n(s)$$

$$= \sum_{n=1}^{N} S_n(s) + \frac{1}{z^2} G(s) G^*(s) \sum_{n=1}^{N} S_n(s) + \frac{1}{z} \sum_{n=1}^{N} \left\{ G(s) e^{-\tau_n s} + \left[G(s) e^{-\tau_n s} \right]^* \right\} S_n(s) \tag{25}$$

The relative mean-square pressure spectrum density of the source without reflection effects is then

$$S_F(s) = \sum_{n=1}^{N} S_n(s) \tag{26}$$

Assume that all sources are of equal strength. Then

$$S_F(s) = NS_n(s) \tag{27}$$

Using equation (10)

$$G(s)e^{-\tau_n s} + \left[G(s)e^{-\tau_n s}\right]^* = Q(s)\left[e^{-\tau_n s + j\delta(s)} + e^{\tau_n s - j\delta(s)}\right]$$

$$= 2Q(s)\cos\left[2\pi f\tau_n - \delta(s)\right] \tag{28}$$

In terms of a one-third-octave spectrum, equation (28) can be easily evaluated if Q(s) and $\delta(s)$ are assumed to be constant in any one-third-octave band using equations (B1) to (B7). Equation (28) is evaluated as follows:

$$\int_{f_a}^{f_b} Q(s)\cos\left[2\pi f\tau_n - \delta(s)\right] df = \frac{Q(f_c)}{2\pi\tau_n}\left\{\sin\left[2\pi f_b\tau_n - \delta(f_c)\right] - \sin\left[2\pi f_a\tau_n - \delta(f_c)\right]\right\} \tag{29}$$

Using the trigonometric identity

$$\sin\omega_b\tau_n - \sin\omega_a\tau_n = 2\cos\frac{(\omega_b + \omega_a)}{2}\tau_n \sin\frac{(\omega_b - \omega_a)}{2}\tau_n \tag{30}$$

and equations (B6) and (B7), we obtain from equation (29)

$$\int_{f_a}^{f_b} Q(s)\cos\left[2\pi f\tau_n - \delta(s)\right] df = \Delta f_c Q(f_c)\cos\left[2\pi f_c\tau_n - \delta(f_c)\right]\frac{\sin(\pi\,\Delta f_c\tau_n)}{\pi\,\Delta f_c\tau_n} \tag{31}$$

If the source spectrum $S_F(s)$ is assumed to be constant over any one-third-octave band the measured one-third-octave spectrum (neglecting atmospheric attenuation) can be obtained by substituting equation (25) into equation (B2) and using equations (10), (27), and (31). Thus,

$$H(f_c)\,\Delta f_c = S_F(f_c)\,\Delta f_c \left\{ 1 + \frac{1}{z^2} Q(f_c)^2 + \frac{2}{N}\frac{Q(f_c)}{Z} \sum_{n=1}^{N} \cos\left[2\pi f_c \tau_n - \delta(f_c)\right] \frac{\sin(\pi\,\Delta f_c \tau_n)}{\pi\,\Delta f_c \tau_n} \right\} \tag{32}$$

where the notation has been changed in that since $s = j2\pi f_c$, parameters hitherto represented as a function of s will henceforth be represented as functions of f_c.

This equation represents the output one-third-octave spectrum $H(f_c)\,\Delta f_c$ as the product of the input one-third-octave spectrum $S_F(f_c)\,\Delta f_c$ and a reflectance factor $\left|T(f_c)\right|^2$, where

$$\left|T(f_c)\right|^2 = 1 + \frac{1}{z^2} Q(f_c)^2 + \frac{2}{N}\frac{Q(f_c)}{z} \sum_{n=1}^{N} \cos\left[2\pi f_c \tau_n - \delta(f_c)\right] \frac{\sin(\pi\,\Delta f_c \tau_n)}{\pi\,\Delta f_c \tau_n} \tag{33}$$

Thus

$$H(f_c)\,\Delta f_c = S_F(f_c)\left|T(f_c)\right|^2 \Delta f_c \tag{34}$$

Equation (34) can be interpreted in terms of well-defined single input, which is from a stationary random process having a one-third-octave spectrum $S_F(f_c)\,\Delta f_c$ and an output that belongs to a stationary random process having a one-third-octave spectrum $H(f_c)\,\Delta f_c$.

Reflected-Ray Transfer Function

The reflected-ray transfer function $G(f_c)$ (where $G(f_c) = Q(f_c)e^{j\delta(f_c)}$, eq. (10)) must be specified to calculate the reflectance $\left|T(f_c)\right|^2$ (eq. (33)). If the reflected-ray transfer function depended only on the acoustic impedance of the ground surface, its value might be measured directly, using the method discussed in reference 45, or calculated based on the assumption that the ground acoustical properties are similar to the measured properties of some material (refs. 46 to 49). But the problem of evaluating the reflecting properties of a ground surface and using the results with an extended source such as is produced by an engine or nozzle is so complicated that common experimental solutions to the problem are either to apply a sound absorbing material to the reflecting surface (refs. 50 and 51) or to use flush mounted microphones (refs. 52

and 53). The problem becomes complicated when the source is an externally blown flap, because, for short wavelengths reflections from the wing-flap and ground, surfaces may become randomized such that the interference effect becomes to some extent indeterminate. Then the reflected-ray transfer function may be determined by a scattering of the incident wave.

Specific factors important in evaluating the reflected-ray transfer function are (1) the variation of the surface impedance with moisture in the soil and vegetable roots in the soil (ref. 45) and (2) the variation of the reflection coefficient C_R with the angle of incidence θ_{inc}. The reflection coefficient is related to the surface impedance and θ_{inc} by

$$C_R(f, \theta_{inc}) = \frac{Z(f) \cos \theta_{inc} - \rho c_o}{Z(f) \cos \theta_{inc} + \rho c_o} \tag{35}$$

where $Z(f)$ is the surface impedance (in general, a complex quantity dependent on frequency) in acoustical ohms times square meter (also called rayl), ρ is the density of air, c_o is the velocity of sound in air ($\rho c_o = 416\ \Omega \cdot m^2$ (MKS rayles)), and θ_{inc} is the angle between the incident ray and the normal to the surface (ref. 44). The absorption coefficient of the ground C_R is related to the reflection coefficient $\alpha(\theta)$ by

$$\left|C_R(f, \theta)\right|^2 = 1 - \alpha(f, \theta) \tag{36}$$

The reflected-ray transfer function $G(f_c)$ would be equal to the reflection coefficient C_R if the reflected-ray transfer function depended only on the ground impedance. Thus,

$$G(f_c) = C_R(f_c, \theta) \tag{37}$$

and the reflected-ray transfer function $G(f_c)$ is related to the absorption coefficient $\alpha(f_c, \theta)$

$$\left|G(f_c)\right|^2 = \left[Q(f_c)\right]^2 = \left|C_R(f_c, \theta)\right|^2 = 1 - \alpha(f_c, \theta) \tag{38}$$

The reflected-ray transfer function $G(f_c)$ is assumed to be independent of frequency. This assumption is made, first, because impedance tube measurements of the normal absorption coefficient $\alpha_N = \alpha(f, 90^o)$ of sharp sand over a frequency range from 200 to 1000 hertz for a moisture content ranging from 0 to 10 percent indicated that the normal absorption coefficient was not strongly dependent on frequency at a given moisture

content (ref. 45). However, the normal absorption coefficient changed with moisture content. Thus equation (38) indicates that under some conditions certain materials have reflected-ray transfer function magnitudes that do not change with frequency but do change with moisture content. The reflected-ray transfer function is assumed to be independent of frequency, secondly, because of a lack of ground surface impedance data at the site of the EBF turbofan engine experiment and because of the possibility of scattering being an important factor in the multiple reflection model introduced to deal with the problems created by an extended EBF source. Thus

$$G(f_c) = Qe^{j\delta} \tag{39}$$

where the constants Q and δ are now frequency independent.

CALCULATED SOUND PRESSURE LEVEL

The calculated sound pressure level equation used herein is formed by first combining the one-third-octave lossless sound-pressure equation (eq. (1)) with a spectral density equation (eq. (F1)) and equations for the reflection correction (eqs. (33) and (39)). Thus

$$SPL''_{cal}\left[f_c(l)\right] = 10 \log_{10}\left\{S_F\left[f_c(l)\right] \left|T\left[f_c(l)\right]\right|^2 \Delta f_c(l)\right\}$$

$$= SPL^+(l) + 10 \log_{10}\left|T\left[f_c(l)\right]\right|^2$$

$$= 10 \log_{10} \left(\left[10^{(OASPL_p^+/10)} \Delta f_c(l) \frac{D_e}{V_e} \right] \left\{ \frac{\left| a_o \prod_{i=1}^{M_a} \left[\Omega(l) - a_i\right] \right|^2}{\left| \prod_{k=1}^{N_b} \left[\Omega(l) - b_k\right] \right|^2} \right\} \left\{ 1 + \frac{Q^2}{z^2} \right.\right.$$

$$\left.\left. + \frac{2}{z} \frac{Q}{N} \sum_{n=1}^{N} \cos\left[2\pi f_c(l)\tau_n - \delta\right] \frac{\sin\left[\pi \Delta f_c(l)\tau_n\right]}{\pi \Delta f_c(l)\tau_n} \right\} \right) \tag{40}$$

where $OASPL_p^+$ is a parameter representing the lossless overall sound pressure level, a_o is spectral density normalization parameter, a_i:i = 1, . . ., M_a and b_k:k = 1, . . ., N_b are complex parameters that aid in determining the shape of the spectral density curve, Q is a frequency independent parameter that determines the amount the reflected wave interferes with direct wave, and δ is a frequency independent parameter indicating the phase angle change in the reflected wave relative to the direct wave. This spectrum must then be corrected for atmospheric attenuation. The correction used in this report is based on that in reference 54. Let $A_{tot}(f_c, r)$ represent this correction; then

$$SPL_{cal}\left[f_c(\ell)\right] = SPL''_{cal}\left[f_c(\ell)\right] + A_{tot}\left[f_c(\ell), r\right]$$

$$= SPL^+(\ell) + 10 \log_{10} \left|T\left[f_c(\ell)\right]\right|^2 + A_{tot}\left[f_c(\ell), r\right] \tag{41}$$

Equation (41) will be used to represent the measured spectrum. The calculation method used to identify parameters that will enable equation (41) to fit a one-third-octave band SPL spectrum will be discussed next.

CALCULATION METHOD

A computer method is used (1) to find an empirical curve that represents the measured SPL corrected for reflection effects and atmospheric absorption and (2) to conduct a numerical evaluation of the effect of reflections on the measured SPL. This is achieved by using the computer to determine parameters such that a calculated reflection correction and a calculated lossless SPL spectrum are adjusted to give a minimum least-square error when compared with a measured SPL spectrum after taking into account atmospheric absorption.

The computer program is initiated by first selecting parameters that define a mathematical model for the ground reflection effect and for the sound spectrum and then, the initial values of the parameters, which the computer adjusts. The adjusted parameters are subject to certain constraints. These constraints are used to define cost and penalty functions (refs. 55 and 56) to assure that the final parameters satisfy the constraints.

Cost Function

The computer program is used to calculate the SPL_{cal} parameters (a_i, b_k, $OASPL_p^+$, Q, δ). The program is designed to minimize a cost function C_e by adjusting the

parameters. Actually, the computer program adjusts the parameters to minimize a quantity C_{tot}, which is the sum of the cost function C_e and a penalty function C_{pen}.

The cost function C_e is the weighted sum of the squares of the differences between the measured SPL_m and calculated SPL_{cal} (eqs. (40) and (41)) sound pressure level at each frequency $f_c(l)$. Thus,

$$C_e = \sum_l \alpha_l \left\{ SPL_m\left[f_c(l)\right] - SPL_{cal}\left[f_c(l)\right] \right\}^2 \tag{42}$$

The total cost function C_{tot} is thus defined as

$$C_{tot} = \sum_l \alpha_l \left\{ SPL_m\left[f_c(l)\right] - SPL_{cal}\left[f_c(l)\right] \right\}^2 + C_{pen} \tag{43}$$

The penalty function, C_{pen}, is discussed next.

As mentioned previously the parameters are subject to constraints. (See eq. (2) for the constraint on $OASPL_p^+$ and eq. (5) for constraints on a_i and b_k.) To insure compliance with these constraints a "penalty function" C_{pen} is added to the cost function. The penalty function increases the cost when an associated constraint is violated. Since the computer iteratively adjusts the parameters to minimize the total cost function, parameters violating a constraint are not reached by the adjustment process.

The constraints arise as follows. The parameters in equation (5) have limits. They must be chosen so that the poles b_k and the zeroes a_i of the function $\varphi(\Omega)$ have negative real parts and positive imaginary parts. Also, the values of the parameter $OASPL_p^+$ must satisfy equation (2); thus

$$OASPL_p^+ = 10 \log_{10} \sum_l \left\{ 10^{\left[SPL_{cal}^+(l)/10\right]} \right\} = OASPL_{cal}^+ \tag{44}$$

The penalty function has the following characteristics. If the real part of a root of $a(\Omega)$ or $b(\Omega)$ is less than zero, or the imaginary part of a root of $a(\Omega)$ or $b(\Omega)$ is greater than zero, the individual penalty is zero. If the real part of a root of $a(\Omega)$ or $b(\Omega)$ is greater than or equal to zero or the imaginary part of a root of $a(\Omega)$ or $b(\Omega)$ is less than or equal to zero, the individual penalty is equal to the square of the real part of the root or the imaginary part of the root. The total penalty is the sum of the indi-

vidual penalties for all the roots plus the weighted sum of the squares of the differences of the parameter value of the reflection corrected unattenuated overall sound pressure level $OASPL_p^+$ and the calculated value of the reflection corrected unattenuated overall sound pressure level $OASPL_{cal}^+$ (based on eq. (43)). Thus,

$$C_{pen} = \sum_{i=1}^{M_a} \delta_a(i)\left[Re\, a_i\right]^2 + \sum_{k=1}^{N_b} \delta_b(k)\left[Re\, b_k\right]^2 + \sum_{i=1}^{M_a} \delta_c(i)\left[Im\, a_i\right]^2 + \sum_{k=1}^{N_b} \delta_d(k)\left[Im\, b_k\right]^2 + \beta\left(OASPL_{cal}^+ - OASPL_p^+\right)^2 \tag{45}$$

where

$$\delta_a(i) = \begin{cases} 1 & Re\, a_i \geq 0 \\ 0 & \text{Otherwise} \end{cases} \tag{46}$$

$$\delta_b(k) = \begin{cases} 1 & Re\, b_k \geq 0 \\ 0 & \text{Otherwise} \end{cases} \tag{47}$$

$$\delta_c(i) = \begin{cases} 1 & Im\, a_i \leq 0 \\ 0 & \text{Otherwise} \end{cases} \tag{48}$$

$$\delta_b(k) = \begin{cases} 1 & Im\, b_k \leq 0 \\ 0 & \text{Otherwise} \end{cases} \tag{49}$$

Optimization

The problem of minimizing a nonlinear function like the cost function given by equation (43) can be solved by search techniques. These techniques consist of systematic procedures for varying the cost function parameters until a minimum value of the cost function is found. The basic methods available are discussed in references 55 and 56. To provide flexibility in the choice of the order of equation (15) (i.e., the number of

terms M_a and N_b), and to accommodate a penalty function, a search technique that does not require evaluation of derivatives was chosen. The search technique was that of Powell (ref. 57). The computer program was adapted from reference 58. The optimization procedure has previously been applied successfully to a similar identification problem (ref. 59).

For modeling acoustic data choosing the number of terms in the linear system power density spectrum function (i.e., the model order) is a serious problem. The selection of a low-order model limits the frequency range over which the function resembles the data. The selection of a high-order model causes the function to adjust to all the variations in the measured data including those due to the reflection effects. The effect of adjusting the model order (i.e., changing the number of poles N_b or the number of zeroes M_a in eq. (40)) on the minimum residual error provides some guide as to the appropriateness of the model. Thus the variation of the minimum cost obtained for different values of N_b and M_a helps determine the best values to use. Various schemes besides the test of the residual error have been proposed to help select the model order for identification problems (ref. 60).

The number of poles N_b selected for the model was one. The number of zeroes M_a was three. These values were selected specifically for the data discussed in the application section of this report.

RESULTS

APPLICATION TO MEASURED DATA

The method for finding the PSD^{+}_{cal} function and the parameters Q and δ was applied to data from a large scale externally blown flap. The scope of this report does not include interpretation of these data, since they are interpreted and discussed in reference 1.

An N independent point source model consisting of five point sources of equal strength was selected to represent the data which the procedure was applied to fit. One point source was chosen to be on the engine axis at the nozzle exit. Two other point sources were assumed to be 36.6 centimeters (1.2 ft) vertically above and below this point, and two more point sources were assumed to be vertically displaced 73.2 centimeters (2.4 ft) above and below the engine centerline. Calculations show that the use of more than five point sources does not appreciably affect the magnitude of the cancellations and reinforcements so long as the total maximum vertical displacement is the same.

Test Conditions

The test data to be evaluated were obtained using a coannular nozzle. The flaps were set at 0°-20°-40° flap angle pattern, meaning that the leading flap was not deflected, the trailing edge of second flap was deflected 20° from the wing reference chord line, and the trailing edge of the third flap was deflected 40° This is referred to as the takeoff flap condition. A schematic diagram of the flap configuration is shown in figure 1(b). The nozzle axis was at a 5° angle with respect to the reference chord line of the wing. More characteristics of the test configuration are given in table 1.

The microphones (fig. 1(c)) were placed at a radius of 30.48 meters (100 ft) and were at the engine centerline level, which was 2.74 meters (9 ft) above the ground. This is only the nominal height, since the ground at the site sloped slightly. The microphone angles from the engine inlet ccnsidered in this report are 0°, 20°, 40°, 60°, 70°, 80°, 90°, 100°, 120°, and 140°. Most emphasis is placed on the 100° microphone location since data from three microphones at different heights (1.37, 2.74, and 5.49 m (4.5, 9, and 18 ft)) were measured at this position. More details of the test and turbofan engine are available in references 1 to 3.

Test Data

Representative one-third-octave SPL plots of the data from this externally blown flap (EBF) turbofan engine configuration are shown in figure 2. The SPL data selected are from microphones at 20°, 90°, 100°, and 120° for the maximum velocity test.

The plots show that at frequencies above 4000 hertz engine machinery noise sources are probably having an effect on the data. This assumption is also based on other EBF data presented in references 13 and 14. Therefore, only the SPL data at frequencies from 50 to 3150 hertz are used in the following discussion.

From equation (40) the first cancellation due to the direct and reflected waves being 180° out of phase for a single point source and a hard surface ($Q = 1$, $\delta = 0$), would occur at a frequency

$$f_r = \frac{c_o}{2(s_2 - s_1)} \tag{50}$$

and the second reinforcement due to the direct and reflected wave being in phase would occur at $2f_r$. For the test facility shown in figure 1, f_r is within the 315-hertz one-third-octave band when the microphones are at 2.74 meters (9 ft). The first cancellation is indicated on the SPL plots by C_1 and the second reinforcement by R_2 (R_1 is at

0 hertz). For microphones at 1.37 meters (4.5 ft) the first cancellation is within the 630-hertz band, and the second reinforcement is within the 1250-hertz band. For microphones at 5.48 meters (18 ft) the first cancellation is within the 160-hertz band, and the second reinforcement is within the 315-hertz band.

Examination of the SPL at the 20° microphone shown in figure 2(a) indicates a cancellation at 315 hertz. A cancellation at 315 hertz is also apparent in the SPL from the 90° microphone shown in figure 2(b). No cancellations are indicated in the SPL at the 100° microphone shown in figure 2(c) or the 120° microphone shown in figure 2(d). If the ground is assumed uniform, the ground impedance concept would give equal interference effects at all angles. The data plots indicate that this is not the case. The concept that a reflected-ray transfer function could vary with view angle and cause the different interference effects at different microphones is an explanation for these measurements. The multiple reflection model is emphasized herein, since it is known that the relative position of the flaps to the hypothesized N independent sources on the trailing edge of the third flap changes with the angle of observation, while the noise source azimuthal directivity variation, the nature of the dominate noise source and the interaction of the various noise sources are not known currently.

Effective diameter and effective velocity are used in the conversion of SPL^{+} to the PSD^{+}. The effective diameter is calculated as follows:

$$D_e = \left[\frac{4}{\pi}\left(A_{fan} + A_{core}\right)\right]^{1/2} \tag{51}$$

The effective velocity V_e is calculated from

$$V_e = \left(\frac{A_{fan}V_{fan}^6 + A_{core}V_{core}^6}{A_{fan} + A_{core}}\right)^{1/6} \tag{52}$$

where the velocities used are obtained by isentropic expansions from total to ambient conditions.

These relations (eqs. (51) and (52)) are based on the data described in references 7 and 8. For the data of reference 8, these relations applied reasonably well to the simple nozzle-flap configuration tested using a convergent and a coannular nozzle. The tested configuration of reference 8 was based on one of the double slotted external flow jet flap configurations developed by the NASA Langley Research Center. Also in reference 8, a scaling procedure is described that can be used to estimate full-scale blown flap noise from small scale data.

Calculation Procedure

Figure 3 shows a diagram of the computer calculation method. The input information consists of the following: (1) the measured sound spectrum SPL_m, (2) the constants defining the spectrum density equation order (M_a and N_b), (3) the constants used to convert from Strouhal number to frequency (D_e and V_e), (4) the constants defining the reflection model (N, z, τ_n:n = 1, . . ., N), (5) the initial parameter values ($OASPL_p^+$; a_i:i = 0, . . ., M_a; b_k:k = 1, . . ., N_b; Q; δ), and (6) the atmospheric attenuation correction. The computer program calculates at the start of each iteration step the following quantities using the current set of parameter values: (1) the reflectance ($|T(f_c)|^2$), (2) the mean-square-pressure spectrum density level PSD_{cal}^+, (3) the SPL spectrum without reflection and atmospheric attenuation effects SPL_{cal}^+, (4) the SPL spectrum with atmospheric attenuation and reflection effects SPL_{cal}. Next, the cost function C_e is calculated from equation (42). Then the penalty function C_p is calculated using equations (43) to (48). Last, these two quantities are summed to obtain the total cost C_{tot}. The new total cost is compared with previous values of the total cost to see if another iteration is necessary. The calculations may stop at this point or continue. If the process is to continue, the new total cost and previous values of the total cost are used by the computer to adjust the current parameter values and to obtain new parameter values that will reduce the total cost. These new values are used to initiate a new iteration.

If another iteration is not needed, the procedure terminates. The current values of the parameters $|T(f_c)|^2$, PSD_{cal}^+, SPL_{cal}^+, and SPL_{cal} are then available. Besides these quantities, a mean square pressure spectrum density level based on the measured SPL_m and the calculated reflectance and atmospheric attenuation PSD_m^+ is also calculated. This can be compared with PSD_{cal}^+ to check the accuracy of the curve fit and the ability of the reflectance to account for interference effects.

The process is thus seen to be based on comparing a measured sound spectrum SPL_m with a hypothetical calculated sound spectrum SPL_{cal}. The hypothetical calculated sound spectrum SPL_{cal} is based on two calculated curves: (1) a PSD_{cal}^+ curve and (2) a $|T(f_c)|^2$ curve. These curves are assumed to be independent. The final curve shapes are achieved by the iteration procedure are assumed to model the actual physical values of these quantities.

As mentioned previously one of the first steps is to select the PSD_{cal}^+ model and the values of the PSD_{cal}^+ parameters. This is covered in detail in appendix F. The reflection model parameters τ_n and z are based on the test site geometry. Numerical experimentation indicates that increasing N beyond five does not change the reflectance if the distance between the furthest source and the nozzle exit centerline position is fixed for fixed z, Q, and δ. The value of Q is between zero and one and the initial δ was selected to be 2π.

Comparisons

Initial and final iteration values of SPL_{cal}, SPL^{+}_{cal}, $|T(f_c)|^2$, and PSD^{+}_{cal} are shown in figure 4. Figure 4(a) shows the initial and final hypothetical SPL_{cal} curves. Also for comparison, data for the input sound spectrum SPL_m are shown. Although the initial hypothetical spectrum does not agree with measured spectrum, the computer program was able to adjust the parameters so that the final calculated spectrum is in good agreement. The largest error occurs near 800 hertz.

Figure 4(b) shows the initial and final SPL^{+}_{cal} curves. The final SPL^{+}_{cal} curve has a peak level of 107.16 decibels at 80 hertz.

The initial and final reflectance level curves are compared in figure 4(c); the final value of Q was 0.48. Figure 4(d) shows that the final PSD^{+}_{cal} curve had a peak level value of 4.22 decibels at a Strouhal number of 0.244. At high Strouhal numbers both the initial and final PSD^{+}_{cal} curves have similar slopes.

Figure 4(e) shows PSD^{+} based on correcting the measured data for atmospheric attenuation effects and for reflectance effects. The reflectance effects are corrected using the hypothetical reflectance level curve. The resulting PSD^{+}_{m} curve is compared with the final PSD^{+} curve based on the curve fit PSD^{+}_{cal}. Again, the error is largest near a Strouhal number of 31, which corresponds to 800 hertz. The final calculated PSD^{+}_{cal} curve is in good agreement with the PSD^{+}_{m} curve based on measured data.

In appendix G characteristics of the rational function PSD^{+} and trends of the curve fit values of the $OASPL^{+}_{p}$ parameter are discussed.

REFLECTION CORRECTION

Two aspects of the reflection correction will be covered. The first deals with ability of the method to correct or decrease the cancellations and reinforcements in the SPL_m and the second with the reflected ray transfer function.

Application of Reflectance

The concept to be illustrated is the existence of a hypothetical PSD^{+} curve and a hypothetical reflected ray-transfer impedance at a given angle and/or a given test condition that can be used to calculate the SPL that would be measured by microphones at different heights and distances from the source. The assumption is made that directivity and angle of incidence effects are secondary and may be neglected. The results obtained using the procedure with data measured at the 100^{o} microphone at the highest exit veloc-

ity test condition (V_e = 242.3 m/sec (795 ft/sec)) are shown in figure 5 for three microphone heights. Figure 5 shows a plot of the calculated unaffected sound pressure level SPL^+_{cal} compared with the sound pressure level including reflection effects and atmospheric attenuation SPL_{cal} and the measured sound pressure level SPL_m.

The agreement between the measured data and the calculated SPL_{cal} is good. The cancellations and reinforcements occur at nearly the same frequency and are of similar size in both measured and calculated SPL curves. The error is of the order of 1 decibel at the frequency of maximum cancellation. Moreover, the calculated SPL^+ should provide a satisfactory estimate of the actual SPL^+ since the SPL_m agrees with the SPL_{cal} at different heights.

Reflected-Ray Transfer Function

For the previous case the value of the reflected-ray transfer function coefficients after the cost function was minimized were $Q = 0.1$ and $\delta = 5.94$ radians ($+340^o$). To obtain some idea of how a change in the magnitude of the reflected-ray transfer function Q affects the data, the case shown in figure 5 can be compared with the one shown in figure 6. Figure 6 presents the data and results for a case having a Q value of 0.5. This is the largest value of Q evaluated by the procedure in the study of the data. The maximum cancellation is shown to be about 5 decibels in figure 6 for the Q equal to 0.5. This can be compared with a maximum cancellation of about 2 decibels for the data shown in figure 5, in which $Q = 0.1$.

Values of Q and δ are presented in table II. Since the value of Q indicates the magnitude of the effect of the reflected-ray transfer function on the cancellations and reinforcements, it will be discussed in some detail. Figure 7 shows a plot of Q with angle over the range of velocities used in this study. The general trend shown is that Q is largest from 20^o to 60^o and smallest from 100^o to 120^o.

To explain this, consider that in previous treatments of reflections (refs. 41 to 44), the reflected-ray transfer impedance could be considered to be caused by the ground surface impedance, since only the reflection from the ground plane occurred. The reflection coefficient C_R calculated in reference 44 is equivalent to the reflected-ray transfer function G when only ground reflection is treated. Thus if the ground impedance is assumed to be independent of frequency of equation (35),

$$G = \frac{Z \cos \theta_{inc} - \rho c_o}{Z \cos \theta_{inc} - \rho c_o} = C_R \tag{53}$$

The ground material at the test site at which the EBF data were obtained is uniform in all directions about the wing flap system, and thus the ground impedance at any angle should yield the same value for the reflection coefficient and produce the same reflection effect at each microphone. Since the reflection coefficient depends only on the surface, no change in the effects it produces should occur with changes in microphone angle.

The observed variation of Q thus seems unrelated to the usual reflection coefficient. One hypothesis that explains the observed variation is that multiple reflections occur due to the presence of the flaps. If this is assumed, the multiple reflections that occur to a ray as it travels from the source to a microphone would be different at each microphone. But, due to the geometry they would be similar for all sources in the same vertical line. Thus reflection effects would be expected to be different at different angles.

SUMMARY OF RESULTS

It has been shown that a computer procedure that corrects for cancellations and reinforcements and that provides for a satisfactory curve fit to sound pressure level data can be designed and implemented. The most important results obtained are that

1. A rational polynomial with a first-order numerator and a third-order denominator is a satisfactory analytic expression for the Strouhal normalized pressure spectral density function.

2. The N independent source model of Thomas is satisfactory to use for correcting externally blown flap data obscured by the presence of interference effects of reflections if it is extended to include a reflected-ray transfer function.

The method discussed in this report has been applied successfully to engine-over-the-wing and engine-under-the-wing externally blown flap data (ref. 1) and is applicable to nozzle only data.

A natural extension of this work would be a study of the way the parameters that determine the PSD^+ (lossless Strouhal normalized mean square pressure spectral density level) function vary with angle and velocity. A set of data that provides more information on the low-frequency roll-off characteristics of the PSD^+ should be used. The PSD^+ function parameters found in this report were not studied to determine trends with velocity and angle since most of the data concerned only the high-frequency roll-off portion of the PSD^+ curve.

Lewis Research Center,
National Aeronautics and Space Administration,
Cleveland, Ohio, December 19, 1974,
501-24.

APPENDIX A

SYMBOLS

A_{core}	core area, cm^2 ($in.^2$)
A_{fan}	fan area, cm^2 ($in.^2$)
A_i	zero of $\varphi(s)$, sec^{-1}
$A(s)$	polynomial equation for zeroes of $\varphi(s)$
$A_{tot}(f_c, r)$	atmospheric attenuation, dB
a_i	zero of $\varphi(\Omega)$, dimensionless
$a(\Omega)$	polynomial equation for zeroes of $\varphi(\Omega)$
a_o	a complex number, normalization constant
B_k	pole of $\varphi(s)$, sec^{-1}
$B(s)$	polynomial equation for poles of $\varphi(s)$
b_k	zero of $\varphi(\Omega)$, dimensionless
$b(\Omega)$	polynomial equation for poles of $\varphi(\Omega)$
C_e	cost function, sum of square of error between measured and calculated sound spectra
C_o	constant
C_{pen}	penalty function
$C_R(f, \theta_{inc})$	reflection coefficient
C_{tot}	total cost function
C_1, C_2, C_3	cancellation frequencies
c	a complex number
c_o	velocity of sound, m/sec
D_e	effective diameter, m
E	see eq. (D11)
E_A	see eq. (D12)
E_B	see eq. (D13)
$E\{\}$	expected value of $\{\}$
$F(u, \eta, c)$	Strouhal response function

f	frequency, Hz
f_a	nominal lower one-third-octave band-edge frequency, Hz
f_b	nominal upper one-third-octave band-edge frequency, Hz
f_c	one-third-octave center frequency, Hz
f_o	critical frequency, Hz
f_r	frequency of first cancellation, Hz
$G(s)$	reflected-ray transfer function
$g(\tau)$	reflecting surface's impulse response function
$H(f)$	relative mean-square pressure spectrum density per unit frequency of signal referenced to 2×10^{-5} Pa
$H(f_c)$	one-third-octave relative mean-square pressure spectrum density of signal relative 2×10^{-5} Pa
h_o	microphone height, m (ft)
$h_s(n)$	height of n^{th} source, m
l	one-third-octave band number
M_a	number of numerator $\sigma(\Omega, a_i)$ terms of $\varphi_{real}(\Omega)$ and number of numerator $(\Omega - a_i)$ terms of $\varphi_{cal}(\Omega)$
N	number of independent noise sources
N_b	number of denominator $\sigma(\Omega, b_k)$ terms of $\varphi_{real}(\Omega)$ and number of denominator $(\Omega - b_k)$ terms of $\varphi_{cal}(\Omega)$
OASPL	overall sound pressure level relative to p_r, dB
$OASPL_p^+$	lossless OASPL parametric value, dB
$P(t, \tau_n)$	observed relative pressure, dimensionless
$P(\omega)$	mean-square pressure spectrum density
PSD	Strouhal normalized mean-square pressure spectral density level, dB
PSD^+	PSD without atmospheric absorption and ground reflection effects, dB
PSD^+_{cal}	PSD^+ calculated from formula, dB
PSD^+_m	PSD^+ calculated from measured data, dB
$PSD^+_{real}(\Omega)$	PSD^+ calculated from a real random process spectrum density, dB
$p(t)$	relative pressure perturbation signal referenced to 2×10^{-5} Pa, dimensionless

p_{tot}	total pressure, Pa
$p'(t)$	reflected relative pressure perturbation signal referenced to p_r
p_o	average atmospheric pressure, Pa
p_r	reference pressure 2×10^{-5} Pa (2×10^{-4} μ bar)
Q	magnitude of reflected-ray transfer function
$R_p(\tau)$	relative mean square pressure autocorrelation function referenced to 2×10^{-5} Pa, dimensionless
$R_{tot}(\xi)$	relative mean square pressure autocorrelation function of signal referenced to 2×10^{-5} Pa, dimensionless
R_2, R_3, R_4	reinforcement frequency
r	distance from source to microphone, m (ft)
$S_F(f)$	relative mean square pressure spectrum density per unit hertz of all sources referenced to 2×10^{-5} Pa
SPL	one-third-octave sound pressure level reference to p_r, dB
SPL^+	one-third-octave sound pressure level referenced to p_r that would be measured without atmospheric attenuation and in the absence of reflecting surface, dB
SPL_{cal}	SPL calculated from an equation, dB
SPL_m	SPL measured, dB
St	Strouhal number, $f(D_e/V_e)$
s	$j2\pi f$, $j\omega$
s_1	distance from source to microphone along direct ray path, m
s_2	distance from source to microphone along reflected ray path, m
$\lvert T(f_c)\rvert^2$	reflectance
T_a	averaging time interval, sec
t	time, sec
u	frequency or Strouhal number ratio, dimensionless
V_{core}	core velocity, m/sec
V_e	effective velocity, m/sec (ft/sec)
V_{fan}	fan velocity, m/sec
x	horizontal position of wing relative to engine (see fig. 1(b)), m (ft)

y	vertical position of wing relative to engine (see fig. 1(b)), m (ft)
Z	ground surface impedance, acoustical ohm · m^2 (mks rayl)
z	mean ratio of path length reflected ray traveled to path length direct ray traveled for all N sources
$\alpha(f, \theta_{inc})$	absorption coefficient
α_l	weighting factor, dimensionless
α_{nor}	normal absorption coefficient, $\alpha(f, 90^o)$
α_o	damping constant
β	weighting factor, dimensionless
β_o	constant
Γ	constant
γ	constant, 1/sec
Δf_c	bandwidth at center frequency f_c (0.2316 f_c), Hz
Δp	pressure perturbation, Pa
$\delta_a(i), \delta_b(k)$	see eqs. (46) and (47), dimensionless
$\delta_c(k), \delta_d(k)$	see eqs. (48) and (49), dimensionless
$\delta_{nn'}$	kronecker delta ($n \neq n: \delta_{nn'} = 0$; $n = n': \delta_{nn'} = 1$)
$\delta(s)$	reflected-ray transfer impedance phase factor, radians (deg)
η	frequency response excitation number
θ	angle between mean flow direction and observation direction, deg
θ_{inc}	acoustic ray angle of incidence, deg
μ	normalized time dealy ($\mu = \tau V_e / D_e$)
ρ	density of air, kg/m^2
ρc_o	acoustical impedance of air, 416 acoustical ohm m^2 (416 mks rayl)
$\sigma(\Omega, c)$	function of Strouhal number such that reciprocal of Fourier transform of damped oscillation is proportional to $\sigma(\Omega, c)^2$
σ, τ, ξ	time delays, sec
τ_n	acoustic delay time from source to microphone, sec
φ	spectral density function, dimensionless
Ω	relative angular velocity, $j2\pi f D_e / V_e = j2\pi St$

ω	angular velocity, $2\pi f$, rad/sec

Subscripts:

cal	calculated
e	effective
i	index of roots of numerator of rational function φ
inc	incidence
k	index of roots of denominator of rational function φ
m	measured
n	source index
o	constant
p	parametric
pen	penalty
real	real
tot	total

Superscripts:

*	complex conjugate
+	spectrum with reflection and atmospheric attenuation effects removed
''	spectrum with atmospheric attenuation effects removed
	reflected ray

APPENDIX B

RELATION BETWEEN THE ONE-THIRD-OCTAVE SOUND PRESSURE LEVEL, SPL, AND THE PRESSURE COVARIANCE FUNCTION, $R_p(\tau)$

The one-third-octave sound pressure level spectrum $SPL(\ell)$ is related to the mean-square-pressure spectral density $H(\omega)$ of a stationary random process by

$$SPL(\ell) = 10 \log_{10} \left\{ H\left[f_c(\ell)\right] \Delta f_c(\ell) \right\} \tag{B1}$$

where

$$H\left[f_c(\ell)\right] \Delta f_c(\ell) = \int_{f_a}^{f_b} H(\omega)\, d\omega \tag{B2}$$

and

$$f_c(\ell) = 10^{\ell/10} \tag{B3}$$

$$f_a = 2^{-1/6} f_c \cong 0.8909\, f_c \tag{B4}$$

$$f_b = 2^{1/6} f_c \cong 1.1225\, f_c \tag{B5}$$

$$f_c = (f_a f_b)^{1/2} \cong \frac{(f_a + f_b)}{2} \tag{B6}$$

$$\Delta f_c = 0.2316\, f_c \tag{B7}$$

The mean-square pressure spectral density $H(\omega)$ will be assumed to be defined over the interval from zero to infinity and referenced to a pressure of 2×10^{-5} pascal (2×10^{-4} μbar). Thus it can be related to the mean-square pressure spectrum density defined over the interval from minus infinity to infinity as follows

$$H(\omega) = \frac{2P(\omega)}{p_r^2} \tag{B8}$$

where $0 < \omega < \infty$. The mean-square pressure spectrum density $P(\omega)$ contains the same information as the pressure covariance function, $R_p(\tau)$. The pressure covariance function is calculated by

$$R_p(\tau) = \lim_{T_a \to \infty} \frac{1}{2T_a} \int_{-T_a}^{T_a} \left[p_{tot}(t) - p_o\right]\left[p_{tot}(t + \tau) - p_o\right] dt$$

$$= \lim_{T_a \to \infty} \frac{1}{2T_a} \int_{-T_a}^{T_a} \Delta p(t)\, \Delta p(t + \tau)\, dt$$

For a stationary real random ergodic process, the time autocorrelation function of a sample function of a random process equals the ensemble average (statistical autocorrelation function) of that process. Thus

$$R_p(\tau) = E\left\{(p_{tot} - p_o)^2\right\} = E\left\{(\Delta p)^2\right\} \tag{B9}$$

The expression $E\{\ \}$ denotes taking an ensemble average. However, the statistical autocorrelation can also be used to define the autocorrelation of a complex random pressure processes. Let Δp_1 and Δp_2 be the random variables that refer to the possible values which can be assumed at the time instants t_1 and t_2, respectively, by the sample functions $\Delta p(t)$ of a given complex random pressure process. Then the autocorrelation function is defined as

$$R_p(t_1, t_2) = E(\Delta p_1\ \Delta p_2^*) \tag{B10}$$

where the asterisk denotes the complex conjugate.

If the given random pressure process is stationary, the joint probability distribution for Δp_1 and Δp_2 depends only on the time difference $\tau = t_1 - t_2$. Thus,

$$R_p(\tau) = R_p(t, t - \tau) = E(\Delta p_t\ \Delta p_{t-\tau}^*)$$

Also, the indicated averages are invariant under a translation of the time origin. Now

$$E(\Delta p_t\ \Delta p_{t-\tau}^*) = E(\Delta p_{t'+\tau}\ \Delta p_{t'}^*) = E^*(\Delta p_{t'}\ \Delta p_{t'+\tau}^*) \tag{B11}$$

therefore,

$$R_p(\tau) = R_p^*(-\tau) \tag{B12}$$

Thus the autocorrelation function of a stationary real random process is an even function of τ (ref. 32).

The mean-square-pressure spectrum density $P(\omega)$ is the Fourier transform of the pressure covariance function.

$$P(\omega) = \int_{-\infty}^{\infty} R_p(\tau)e^{-j\omega\tau}\, d\tau \tag{B13}$$

where $-\infty < \omega < \infty$. A function, in order to represent the mean-square pressure spectrum density $P(\omega)$ must be nonnegative and integrable (finite power) (ref. 32). The pressure spectrum density of a real random process must be an even function of frequency. This follows from equation (B13), since for a real process

$$R_p(\tau) = R(-\tau) \tag{B14}$$

(ref. 32, p. 106).

APPENDIX C

ORIGIN OF RATIONAL FUNCTION FORM OF $\varphi(\Omega)$

The spectrum density of a stationary real random physically realizable process can in many cases be represented as a rational function of frequency f:

$$\varphi(s) = \left| \frac{A_o \prod_{i=1}^{M_z} (s - A_i)}{\prod_{k=1}^{N_p} (s - B_k)} \right|^2 = \left| \frac{A(s)}{B(s)} \right|^2 \tag{C1}$$

where s is a function of frequency defined by $s = j2\pi f$ (where $j = \sqrt{-1}$), the zeroes of B(s) (i.e., the N_p poles) are denoted B_k), the zeroes of A(s) (i.e., the M_z zeroes) are denoted A_k, and A_o is a normalization constant defined such that

$$\int_0^\infty \varphi(f)\, df = 1 \tag{C2}$$

(refs. 32 (p. 233), 33 (p. 378), 34 (p. 410), and 35 (p. 187)).

This functional form of the spectral density can be related to a number of physical phenomena. One example is the spectral density of the output from a lumped-parameter linear electric circuit, which is excited with white noise (ref. 32, p. 105). It resembles measured one-dimensional isotropic turbulence energy spectra (ref. 27). This functional form can also be used to describe the spectral density of other stationary random processes (ref. 36). This form could also be used to represent the power spectral density of broad-band aerodynamic noise with and without the presence of solid boundaries (refs. 18, 21, and 23). According to reference 34, any spectra can be approximated sufficiently closely by a rational function of s. Since $\varphi(s)$ is a spectral density, it has particular properties that imply certain restrictions on the number and location of its poles and zeroes. The parameters A_i and B_k must be chosen so that $\varphi(s)$ is a real, even, nonnegative, integrable function of the frequency f whose inverse Fourier transform is a correlation function. The zeroes of A(s)(A_i) and the zeroes of B(s)(B_k) are constrained to have negative real parts. Also, all A_i and B_k with nonzero real parts must occur in conjugate pairs. Another condition is that the degree of the numerator M_z must be less than the degree of the denominator N_p ($N_z < N_p$; ref. 32, p. 233).

The function of Strouhal number $\varphi(\Omega)$ will be assumed to be defined by the Fourier transform of a function of a normalized time delay μ (where $\mu = \tau V_e/D_e$) denoted as $R(\mu)$. Thus

$$\varphi(\Omega) = \int_{-\infty}^{\infty} R(\mu) e^{-\Omega\mu}\, d\mu$$

where

$$\Omega = s\frac{D_e}{V_e} = j2\pi f\frac{D_e}{V_e} = j2\pi St$$

In the Strouhal number domain the function of Strouhal number $\varphi(\Omega)$ will be assumed to be represented by the following rational function of Ω:

$$\varphi(\Omega) = \left| \frac{A_o \prod_{i=1}^{M_z} (\Omega - A_i)}{\prod_{k=1}^{N_p} (\Omega - B_k)} \right|^2 = \left| \frac{A(\Omega)}{B(\Omega)} \right|^2$$

where the zeroes of $A(\Omega)(A_i)$ and the zeroes of $B(\Omega)(B_k)$ are constrained appropriately as mentioned previously in discussion of the function $\varphi(s)$ defined in the frequency domain and A_o is again a normalization constant.

APPENDIX D

SPECTRUM OF A "DAMPED COSINE OSCILLATION"

Let the pressure covariance function $R_p(\tau)$ be represented by a "damped cosine oscillation"

$$R_p(\tau) = \Gamma e^{-\alpha_o|\tau|} \cos \beta_o \tau \tag{D1}$$

Then from equation (B14) the mean square pressure spectrum of $R_p(\tau)$ is

$$P(\omega) = \frac{2\Gamma\alpha}{|\sigma(\omega, c)|^2} \tag{D2}$$

where

$$\sigma(\omega, c) = \frac{(j\omega - c)(j\omega - c^*)}{(j\omega + \sqrt{cc^*})} \tag{D3}$$

$$c = -\alpha_o + j\beta_o \tag{D4}$$

and the asterisk (*) indicates the conjugate relation.

The behavior of the function of ω, $P(\omega)$, for different values of c is more easily discussed if the function is written in terms of dimensionless variables. Let the critical frequency f_o be defined as

$$f_o = \frac{\beta_o}{2\pi} \tag{D5}$$

the frequency ratio u be defined as

$$u = \frac{\omega}{\beta_o} = \frac{2\pi f}{\beta_o} = \frac{f}{f_o} \tag{D6}$$

and the frequency response excitation number as

$$\eta = \left|\frac{\alpha_o}{\beta_o}\right| \tag{D7}$$

Then equation (D2) can be written as

$$P(\omega) = \frac{2\Gamma\,\alpha_o}{\left(\alpha_o^2 + \beta_o^2\right)\left[\frac{\eta^2 + (u-1)^2}{\eta^2 + 1}\right]\left[\frac{\eta^2 + (u+1)^2}{\eta^2 + u^2 + 1}\right]} \tag{D8}$$

This function is commonly plotted logarithmically. Let

$$PSD_{real}(f) = 10 \log_{10}(2\Gamma\,\alpha_o) + C_o - E(u, \eta, c) \tag{D9}$$

where

$$C_o = 10 \log_{10}\left|\frac{1}{c}\right|^2 \tag{D10}$$

$$E(u, \eta, c) = 10 \log_{10}\left[E_A(u, \eta, c) E_B(u, \eta, c)\right] \tag{D11}$$

$$E_A(u, \eta, c) = \left[\frac{\eta^2 + (u-1)^2}{\eta^2 + 1}\right] \tag{D12}$$

$$E_B(u, \eta, c) = \left[\frac{\eta^2 + (u+1)^2}{\eta^2 + u^2 + 1}\right] \tag{D13}$$

The first two terms of equation (D9) determine the level of the PSD function at zero frequency ratio and are independent of frequency. The last term will be referred to as the basic frequency response function. The behavior of $E(u, \eta, c)$ is shown as a function of frequency ratio u for various excitation values η in figure 8 where $-E(u, \eta, c)$ is plotted.

Figure 8 indicates that for η less than 1.0 the value of η determines the sharpness of the peak of $-E(u, \eta, c)$ with smaller values of η producing higher and more narrow peaked curves. As the value of η increases to one the peaks become broad and lower. At high frequencies curves with η less than 1 merge to form a single curve. Curves with η greater than 1 have parallel slopes at high frequencies.

APPENDIX E

BASIC SPECTRAL DENSITY FUNCTION

The particular realization of the spectral density function defined in appendix C will be formulated from the reciprocal of the Fourier transform of a "damped cosine oscillation" derived in appendix D. The resulting formula is

$$\varphi_{real}(St) = \left| \frac{a_o \prod_{i=1}^{M_a} \sigma(\Omega, a_i)}{\prod_{k=1}^{N_b} \sigma(\Omega, b_k)} \right|^2 = \left| \frac{a(\Omega)}{b(\Omega)} \right|^2 \tag{E1}$$

where $M_a < N_b$, the complex numbers a_i and b_k have negative real values and positive or zero imaginary values, and a_o is a normalization constant.

From equations (D5) to (D13) the PSD function can be written in terms of nondimensional parameters u and η as

$$PSD^{+}_{real}(St) = C_o + \sum_{i=1}^{M_a} E(u, \eta, a_i) - \sum_{k=1}^{N_b} E(u, \eta, b_k) \tag{E2}$$

where now the critical Strouhal number is defined as

$$St_o = \frac{\mathcal{Im}(c)}{2\pi} \tag{E3}$$

The quantity $u(c)$ is the Strouhal number ratio defined as

$$u(c) = \frac{St}{St_o(c)} \tag{E4}$$

The quantity η is the Strouhal response excitation constant defined as

$$\eta(c) = \left| \frac{\mathcal{Re}(c)}{\mathcal{Im}(c)} \right| \tag{E5}$$

and

$$C_o = 10 \log_{10} \left| \frac{a_o \prod_{i=1}^{M_a} a_i}{\prod_{k=1}^{N_b} b_k} \right|^2 \qquad \text{(E6)}$$

Thus equation (E1) can be interpreted in terms of the sum of a level determining constant C_o and various curves such as are shown in figure 9.

APPENDIX F

SIMPLIFIED SPECTRAL DENSITY FUNCTION

Equation (E1) is the power spectral density of a real random process. A modification of equation (6), which yields a simpler expression that is equally suitable for curve fitting PSD^+ data will be discussed next. (However, although the new equation can be used to satisfactorily fit a spectral density, it does not represent a power spectral density of a real random process since it is not an even function of frequency.)

The modification consists of dropping the term $(\Omega - c^*)/(\Omega + \sqrt{cc^*})$ from an equation similar to equation (D3) of appendix D in which $j\omega$ is replaced by Ω (as done in appendix C). The equation for the calculated lossless spectral density $\varphi_{cal}(\Omega)$ then can be written as

$$\varphi_{cal}(\Omega) = \left| \frac{a_o \prod_{i=1}^{M_a} (\Omega - a_i)}{\prod_{k=1}^{N_b} (\Omega - b_k)} \right|^2 = \left| \frac{a(\Omega)}{b(\Omega)} \right|^2 \tag{F1}$$

where all the symbols are the same as in equation (E1).

Equation (F1) also can be written in terms of nondimensional parameters as the sum of terms. The equation for the calculated lossless PSD function is then

$$PSD^+_{cal}(St) = C_o + \sum_{i=1}^{M_a} F(u, \eta, a_i) - \sum_{k=1}^{N_b} F(u, \eta, b_k) \tag{F2}$$

where u, η, and C_o are defined by equations (E3) to (E6) and

$$F(u, \eta, c) = 10 \log_{10} E_A(u, \eta, c) \tag{F3}$$

where $E_A(u, \eta, c)$ is defined by equation (D12).

In figure 9 the basic and simplified Strouhal response functions are compared for Strouhal response excitation η values of 0.05 and 5.0. The figure indicates that the two functions have very similar shapes.

Equation (E1) can be made into an even function of frequency by using the absolute value of Ω instead of Ω. Thus

$$\varphi_{real}(\Omega) = \left| \frac{a_o \prod_{i=1}^{M_a} (|\Omega| - a_i)}{\prod_{k=1}^{N_b} (|\Omega| - b_k)} \right|^2 \qquad \text{(F4)}$$

Equation (E4) represents a physically realizable (real random) process. However, since no use of the function at negative frequencies will be made herein, this notation where $|\Omega|$ replaces Ω will be dropped.

APPENDIX G

TRENDS OF RATIONAL FUNCTION AND CURVE FIT PARAMETERS

The following will be discussed: the effect of velocity on PSD^+_{cal}; the variation of PSD^+_{cal} with microphone angle; the effect of the effective exhaust velocity on $OASPL^+_p$; the variation of $OASPL^+_p$ with microphone angle.

Effect of velocity on PSD^+_{cal}. - A series of PSD^+_{cal} curves that pertain to measurements made at 2.74 and 5.48 meters (9 and 18 ft) at the 100^o angle over an effective velocity range of 162.8 to 242.3 meters per second (534 to 795 ft/sec) are shown in figure 10. These PSD^+_{cal} curves are based on data at both microphone heights. The data at the microphone height of 1.37 meters (4.5 ft) were not used in these calculations since they contain irregular variations not shown in the data at 2.74 or 5.48 meters (9 or 18 ft; see fig. 5). Also shown in figure 10 are the corresponding PSD^+_m points.

The functional form used for the PSD^+_{cal} curves is

$$PSD^+_{cal} = 10 \log_{10}\left\{\left|\frac{a_o(\Omega - a_1)}{(\Omega - b_1)(\Omega - b_2)(\Omega - b_3)}\right|^2\right\} \qquad \text{(G1)}$$

Figure 10 shows that equation (G1) fits the data well. The deviation of the data from the empirical curve is less than 1 decibel at most frequencies. The maximum of each curve occurs between Strouhal numbers of 0.25 and 0.35. A problem was encountered in determining the maximum, since the initial Strouhal number for the lower velocity cases is very close to that at which the maximum for the PSD_{cal} curve occurs. In figure 11 the curves shown in figure 10 are plotted together and fall within a narrow band.

The variation of PSD^+_{cal} with angle. - A series of PSD^+_{cal} curves which pertain to measurements made at the maximum effective velocity (V_e = 242.3 m/sec (795 ft/sec)) over a range of angles from 20^o to 120^o is shown in figure 12.

Equation (G1) was used to curve fit the data. Since only data from the microphones at a height of 2.74 meters (9 ft) was available at most angles, the curves shown in figure 12 are based on less data than those in figure 10.

Most of the PSD^+_{cal} curves shown in figure 12 are similar. For instance, they all tend to peak at a Strouhal number between 0.25 and 0.35.

Two importance characteristics of the PSD^+_{cal} curve are the Strouhal number at which it peaks and the peak value. The variation of these two characteristics with microphone angle is shown in figure 13. Here, in order to indicate that the trends

applied to more than one particular case, results based on data from the two highest velocity tests are shown. Note that the peak of the Strouhal curve is calculated from one-third-octave SPL data; thus it can represent only the approximate maximum. Also note that the peak is not as well defined for the 224.6-meter-per-second (737-ft/sec) data as for the 242.3-meter-per-second (795-ft/sec) data since the number of points with Strouhal number smaller than that of the peak is less.

In figure 14 the calculated PSD^{+}_{cal} curves for angles from 40° to 120° of figure 12 are plotted together. This figure shows that all the curves fall within a narrow band.

Effect of jet velocity on $OASPL^{+}_{p}$. - Figure 15 shows the variation of $OASPL^{+}_{p}$ with effective velocity at each angle. The same trends observed in reference 18 are present. The $OASPL^{+}_{p}$ from the microphones between 20° and 100° can be fitted by lines having a sixth power slope. The $OASPL^{+}_{p}$ from the microphones at 120° show a slope closer to eighth power. This is especially apparent at the highest velocities.

These results suggest that the spectrum from the microphones between 20° and 100° is dominated by blown-flap noise, since flap noise is thought to be proportional to the sixth power of the effective velocity and that the microphones at 120° are affected by jet noise, since jet noise is proportional to the effective velocity to the eighth power.

Tabulated results. - To enable the reader to use the actual empirical curves, the coefficients found are listed in table II. Also in the table are values of the cost function C_T, the $OASPL^{+}_{p}$ value, and the reflected-ray transfer function parameters Q and δ. The ranges of each of the parameters seem limited, but they were not analyzed for trends since most of the data used to obtain them contained little information on the low frequency roll off.

REFERENCES

1. Miles, J. H.: Rational Function Representation of Flap Noise Spectra Including Correction for Reflection Effects. Paper No. 74-193, AIAA, Jan.-Feb. 1974.

2. Samanich, N. E.; Heidelberg, L. J.; and Jones, W. L.: Effect of Exhaust Nozzle Configuration on Aerodynamic and Acoustic Performance of an Externally Blown Flap System with a Quiet 6:1 Bypass Ratio Engine. Paper No. 73-1217, AIAA, Nov. 1973.

3. Edkins, D. P.: Acoustically Treated Ground Test Nacelle for the General Electric TF34 Turbofan. General Electric Co. (NACA CR-120915), 1972.

4. Jones, W. L.; Heidelberg, L. J.; and Goldman, R. G.: Highly Noise Suppressed Bypass 6 Engine for STOL Applications. Paper No. 73-1031, AIAA, Oct. 1973.

5. Hayden, R. E.: Noise from Interaction of Flow with Rigid Surfaces: A Review of Current Status of Prediction Techniques. NASA CR-2126, 1972.

6. Fink, Martin R.: Mechanisms of Externally Blown Flap Noise. Paper No. 73-1029, AIAA, Oct. 1973.

7. Dorsch, R. G.; Goodykoontz, J. H.; and Sargent, N. B.: Effect of Configuration Variations on Externally Blown Flap Noise. Paper No. 74-190, AIAA, Jan.-Feb. 1974.

8. Dorsch, R. G.; Kreim, W. J.; and Olsen, W. A.: Externally-Blown-Flap Noise. Paper 72-129, AIAA, Jan. 1972.

9. Reshotko, M.; Goodykoontz, J. H.; and Dorsch, R. G.: Engine Over-the-Wing Noise Research. Paper No. 73-631, AIAA, July 1973.

10. Howes, Walton L.: Similarity of Far Noise Fields of Jets. NASA TR R-52, 1959, pp. 132-134.

11. Howes, Walton L.: Similarity of Near Noise Fields of Subsonic Jets. NASA TR R-94, 1961.

12. Williams, T. J.; Ali, M. R. M.; and Anderson, J. S.: Noise and Flow Characteristics of Coaxial Jets. J. Mech. Eng. Sci., vol. 11, no. 2, Apr. 1969, pp. 133-142.

13. Olsen, William A.; Miles, Jeffrey H.; and Dorsch, Robert G.: Noise Generated by Impingement of a Jet Upon a Large Flat Board. NASA TN D-7075, 1972.

14. Olsen, William A.; Dorsch, Robert G.; and Miles, Jeffrey H.: Noise Produced by a Small-Scale Externally Blown Flap. NASA TN D-6636, 1972.

15. Chase, David M.: Sound Radiated by Turbulent Flow off a Rigid Half-Plane as Obtained from a Wavevector Spectrum of Hydrodynamic Pressure. J. Acoust. Soc. Am., vol. 52, no. 3, pt. 2, 1972, pp. 1011-1023.

16. Clark, P. J. F.; and Ribner, H. S.: Direct Correlation of Fluctuating Lift with Radiated Sound for an Airfoil in Turbulent Flow. J. Acoust. Soc. Am., vol. 46, no. 3, pt. 2, 1969, pp. 802-805.

17. Crighton, D. G.; and Leppington, F. G.: Scattering of Aerodynamic Noise by a Semi-Infinite Compliant Plate. J. Fluid Mech., vol. 43, pt. 4, Oct. 1970, pp. 721-736.

13. Curle, N.: The Influence of Solid Boundaries Upon Aerodynamic Sound. Proc. Roy. Soc. (London), vol. 231, 1955, pp. 505-521.

19. Hersh, A. S.; and Meecham, W. C.: Sound Directivity Pattern Radiated by Small Airfoils. J. Acoust. Soc. Am., vol. 53, no. 2, 1973, pp. 602-606.

20. Kraichnan, Robert H.: Pressure Fluctuations in Turbulent Flow Over a Flat Plate. J. Acoust. Soc. Am., vol. 28, no. 3, May 1956, pp. 378-390.

21. Meecham, William C.: Surface and Volume Sound from Boundary Layers. J. Acoust. Soc., Am., vol. 37, no. 3, Mar. 1965, pp. 516-522.

22. Phillips, O. M.: On the Aerodynamic Surface Sound From a Plane Turbulent Boundary Layer. Proc. Roy. Soc. (London), vol. A234, 1956, pp. 327-335.

23. Powell, Alan: Aerodynamic Noise and the Plane Boundary. J. Acoust. Soc. Am., vol. 32, no. 8, Aug. 1960, pp. 982-990.

24. Sharland, I. J.: Sources of Noise in Axial Flow Fans. J. Sound Vib., vol. 1, no. 3, Jul. 1964, pp. 302-322.

25. Siddon, Thomas E.: Surface Dipole Strength by Cross-Correlation Method. J. Acoust. Soc. Am., vol. 53, no. 2, 1973, pp. 619-633.

26. Vecchio, E. A.; and Wiley, C. A.: Noise Radiated from a Turbulent Boundary Layer. J. Acoust. Soc. Am., vol. 53, no. 2, 1973, pp. 596-601.

27. Hinze, J. O.: Turbulence; An Introduction to its Mechanism and Theory. McGraw-Hill Book Co., Inc., 1959.

28. Corcos, G. M.: Resolution of Pressure in Turbulence. J. Acoust. Soc. Amer., vol. 35, no. 2, Feb. 1963, pp. 192-199.

29. Corcos, G. M.: The Resolution of Turbulent Pressures at the Wall of a Boundary Layer. J. Sound. Vib., vol. 6, no. 1, Jul 1967, pp. 59-70.

30. Schloemer, Howard H.: Effects of Pressure Gradients on Turbulent-Boundary Layer Wall-Pressure Fluctuations. J. Acoust. Soc. Amer., vol. 42, no. 1, 1967, pp. 93-113.

31. Bendat, Julius S.; and Piersal, Allan G.: Measurement and Analysis of Random Data. John Wiley & Sons, Inc., 1966.

32. Davenport, Wilbur B., Jr.; and Root, William L.: An Introduction to the Theory of Random Signals and Noise. McGraw-Hill Book Co., Inc., 1958.

33. Lee, Yuk W.: Statistical Theory of Communication. John Wiley & Sons, Inc., 1960.

34. Papoulis, Athonasios: Probability, Random Variables, and Stochastic Processes. McGraw-Hill Book Co., Inc., 1965.

35. Van Trees, Harry L.: Detection, Estimation, and Modulation Theory. John Wiley & Sons, Inc., 1968.

36. Yoglom, A. M.: Stationary Random Functions. Prentice-Hall, Inc., 1962.

37. Dorf, Richard C.: Modern Control Systems. Addison-Wesley Publishing Co., 1967.

38. Octave, Half-Octave, and Third-Octave Band Filter Jets. Sl. 11-1966, ANSI.

39. Thomas, P.: Acoustic Interference by Reflection: Application to the Sound Pressure Spectrum of Jets. AGARD Aircraft Engine Noise and Sonic Boom. AGARD-CP-24, 1969.

40. Mariano, Sulmo: Ground Effect of a Plane Uniform Sound Source Distribution. D6-22600TN, Boeing Co., 1969.

41. Howes, Walton L.: Ground Reflection of Jet Noise. NASA TR R-35, 1959.

42. Franken, Peter A.: A Theoretical Analyses of the Field of a Random Noise Source Above an Infinite Plane. NACA TN-3557, 1955.

43. Hoch, R.; and Thomas, P.: The Influence of Reflections on the Sound-Pressure Spectra of Jets. NASA TT F-12, 246, 1969.

44. Morse, Philip M.; and Ingard, K. U.: Theoretical Acoustics. McGraw-Hill Book Co., Inc., 1968.

45. Dickinson, P. J.; and Doak, P. E.: Measurements of the Normal Acoustic Impedance of Ground Surfaces. J. Sound Vib., vol. 13, no. 3, Nov. 1970, pp. 309-322.

46. Delany, M. E.; and Bazley, E. N.: A Note on the Effect of Ground Absorption in the Measurement of Aircraft Noise. J. Sound Vib., vol. 16, no. 3, June 1971, pp. 315-322.

47. Delany, M. E.; and Bazley, E. N.: Acoustical Characteristics of Fibrous Absorbent Materials. NPL-AERO-Ac-37, National Physical Lab., 1969.

48. Oncley, P. B.: Propagation of Jet Engine Noise Near a Porous Surface. J. Sound Vib., vol. 13, no. 1, Sept. 1970, pp. 27-35.

49. Powell, John G.; and Van Houten, John J.: Techniques for Evaluating the Sound Absorption of Materials at High Intensities. NASA CR-1698, 1971.

50. Moore, C. J.: A Solution to the Problem of Measuring the Sound Field of a Source in the Presence of a Ground Surface. J. Sound Vib., vol. 16, no. 2, May 1971, pp. 269-282.

51. Olsen, W. A.; Gutierrez, O. A.; and Dorsch, R. G.: The Effect of Nozzle Inlet Shape, Lip Thickness, and Exit Shape and Size on Subsonic Jet Noise. NASA TM X-68182, 1973.

52. McKaig, M. B.: Use of Flush-Mounted Microphones to Acquire Free-Field Data. Paper 74-92, AIAA, Jan.-Feb. 1974.

53. Atvars, J.; Paynter, G. C.; Walker, D. Q.; and Wintermeyer, C. F.: Development of Acoustically Lined Ejector Technology for Multitube Jet Noise Suppressor Nozzles by Model and Engine Tests Over a Wide Range of Jet Pressure Ratios and Temperatures. NASA CR-2382, 1974.

54. Evans, L. B.; and Sutherland, L. C.: Absorption of Sound in Air. WR 70-14, Wyle Labs. (AD-710291; AROD-8725-2-E), 1970.

55. Aoki, Masano: Introduction to Optimization Techniques. The MacMillan Co., 1971.

56. Pierre, Donald A.: Optimization Theory with Applications. John Wiley & Sons, Inc., 1969.

57. Powell, M. J. D.: An Efficient Method for Finding the Minimum of a Function of Several Variables Without Calculating Derivatives. Computer Journal, vol. 7, no. 2, Jul. 1964, pp. 155-162.

58. Shapiro, Miriam S.; and Goldstein, Max: A Collection of Mathematical Computer Routines. NYO-1480-14, New York University, 1965.

59. Miles, Jeffrey H.: Computer Method for Identification of Boiler Transfer Functions. NASA TM X-2436, 1971.

60. Gustavsson, I.: Comparison of Different Methods for Identification of Industrial Processes. Automatica, vol. 8, no. 2, Mar. 1972, pp. 127-142.

TABLE I. - EXPERIMENTAL CONDITIONS FOR TEST OF WING FLAP SYSTEM BLOWN BY TURBOFAN ENGINE WITH COANNULAR NOZZLE AND TAKEOFF FLAP SETTINGS OF 0^{o}, 20^{o}, 40^{o}

[Horizontal position of wing, 30.48 cm (12 in.); vertical position of wing, 104.14 cm (41 in.); fan area, 5096.8 cm^2 (790 $in.^2$); core area, 1812.9 cm^2 (281 $in.^2$); diameter, 93.8 cm (3.077 ft); distance from source to microphone, 30.48 m (100 ft); microphone height,[a] 2.74 m (9 ft).]

Core velocity, V_{core}		Fan velocity, V_{fan}		Effective velocity, V_e		Ambient temperature		Humidity, %
m/sec	ft/sec	m/sec	ft/sec	m/sec	ft/sec	^{o}C	^{o}F	
263.7	865	231.6	760	242.3	795	11.67	53	54.9
236.2	775	219.5	720	224.6	737	12.22	54	53.2
216.4	710	207.3	680	210.0	689	12.22	54	53.2
193.5	635	192.0	630	192.3	631	11.67	53	57.6
157.0	515	164.6	540	162.8	534	11.67	53	54.9

[a]At 100^{o} microphones were also at heights 1/2 h_o and 2 h_o.

TABLE II. - PARAMETERS CALCULATED FOR EMPIRICAL EQUATION (G1)

Effective velocity, V_e, m/sec	Total cost function, C_{tot}	a_o		a_1		b_1		b_2		b_3		Overall sound pressure level, OASPL	Magnitude of reflected-ray transfer function, Q	δ
		Re	*Im*	*Re*	*Im*	*Re*	*Im*	*Re*	*Im*	*Re*	*Im*			
Microphone angle, 0°														
242.3	0.159	419	375	-1.37	1.06	-252	191	-2.13	1.29	-0.69	1.59	108.2	0.206	8.4
224.6	.179	465	375	-1.20	.98	-248	195	-2.14	1.47	-.712	1.5	106.2	.051	7.3
210	.22	563	356	-1.09	.975	227	259	-2.0	1.65	-.693	1.48	104.8	.002	5.98
192.3	.31	480	567	-.431	.944	-198	285	-2.04	1.3	-.592	1.5	102.8	.13	6.28
162.8	.36	644	538	-.0815	.96	-199	265	-2.28	1.14	-.0836	1.14	99.63	.117	6.28
Microphone angle, 20°														
242.3	0.0215	469	371	-1.18	1.14	-254	895	-2.37	1.33	-0.748	1.5	111.7	0.518	0.574
224.6	.018	456	375	-1.28	1.14	-255	113	-2.26	1.39	.78	1.51	109.7	.483	5.72
210	.036	465	375	-1.24	1.07	-256	109	2.3	1.38	-.718	1.39	108.1	.425	5.65
192.3	.368	548	403	-1.097	1.30	-186.4	266.3	-1.97	.832	.531	1.55	106.82	.118	6.28
162.8	.144	457	517	-.7	.91	-238	154	-2.35	1.63	-.578	1.33	102.1	.378	5.65
Microphone angle, 40°														
242.3	0.374	418	378	-1.35	1.17	-262	-629	-2.34	1.59	-0.77	1.51	113.7	0.489	5.75
224.6	.0388	411	379	-1.46	1.33	-256	-72.8	-2.32	1.53	-.746	1.47	111.6	.405	5.71
210	.043	449	375	-1.36	1.13	-253	-95	-2.37	1.63	-.726	1.39	109.4	.398	5.69
192.3	.047	421	378	-1.46	1.033	-263.6	-79.3	-2.38	1.8	-.752	1.43	107.6	.401	5.75
162.8	.057	428	372	-1.53	.890	-265	-92.9	-2.39	2.3	-.78	1.42	103.7	.417	5.61
Microphone angle, 60°														
242.3	0.019	448	375	-1.24	1.041	-261.2	-29.86	-2.39	1.33	-0.758	1.50	114.7	0.483	5.66
224.6	.0249	436	389	-1.26	1.2	-250	-55	-2.39	1.03	-.72	1.47	112.3	.352	5.82
210	.048	459	375	-1.34	1.19	-254	-62	-2.36	1.28	-.698	1.39	110.44	.372	5.73
192.3	.0536	499	375	-1.13	1.33	-225	-116	-2.63	.874	-.512	1.46	108.1	.315	6.28
162.8	.07	512	345	-1.42	1.35	-233	-111.3	-2.49	.988	-.213	1.27	104.1	.205	6.28
Microphone angle, 70°														
242.3	0.034	598	365	-0.81	1	-248	-328	-2.95	0.57	-0.525	1.54	113.8	0.239	6.28
224.6	.0365	562	331	-.96	1.15	-234	-96.8	-2.79	.646	-.552	1.61	111.8	.254	↓
210	.0477	520	345	-1.05	1.09	-241	-91.1	-2.55	.843	-.58	1.42	110.46	.198	
192.3	.054	503.7	350.3	-1.23	1.07	-245	-100	-2.4	1.126	-.606	1.33	108.18	.148	
162.8	.072	500	345	-1.4	1.12	-244.4	-109.1	-2.42	1.45	-.314	1.22	104.48	.06138	

TABLE II. - Concluded. PARAMETERS CALCULATED FOR EMPIRICAL EQUATION (G1)

Effective velocity, V_e, m/sec	Total cost function, C_{tot}	a_o		a_1		b_1		b_2		b_3		Overall sound pressure level, OASPL	Magnitude of reflected-ray transfer function, Q	δ
		Re	Im	Re	Im	Re	Im	Re	Im	Re	Im			
Microphone angle, 80°														
242.3	0.0356	586	559	-0.538	0.896	-241	-95.1	-3.35	0.597	-0.512	1.45	114.25	0.259	6.28
224.6	.0411	620	339	-.691	.955	-231.2	-113	-2.96	.558	-.483	1.51	112.36	.224	
210	.055	596	344	-.714	1.05	-226	-110	-2.88	.491	-.475	1.52	110.4	.244	
192.3	.073	548	354	-.978	.961	-244	-95.9	-2.61	1.06	-.523	1.31	108.5	.143	
162.8	.082	558	352	-1.21	1.02	-246.2	-84.8	-2.52	1.26	-.188	1.14	104.7	.128	
Microphone angle, 90°														
242.3	0.008	499.7	374	-0.71	0.674	-258	672	-2.5	2.36	0.83	1.28	113.8	0.302	5.73
224.6	.0123	476	370	-.827	.68	-264	9.8	-2.5	2.26	-.828	1.3	111.57	.287	5.71
210	.0145	499.6	374	-.94	.78	-258	-33.6	-2.57	2.17	-.764	1.28	109.4	.269	5.47
192.3	.0472	516	370	-.92	.84	-253	-48.68	-2.73	1.95	-.613	1.26	107	.0988	6.28
162.8	.056	501	368	-1.09	.814	-254.5	-68.9	-2.53	2.09	-.535	1.22	102.86	.0964	6.28
Microphone angle, 100°														
242.3	0.00872	472	380	-0.768	0.694	-262	106	-2.31	2.36	-0.809	1.34	114.2	0.0997	5.94
224.6	.0123	457	375	-.732	.674	-259	59	-2.39	2.51	-.832	1.29	111.2	.139	6.14
210	.0138	491	374	-.909	.782	-253	99.6	-2.47	2.62	-.703	1.18	108.9	.0731	6.21
192.3	.01	503	376	-.938	.747	259	51.86	-2.56	2.39	-.736	1.21	106.1	.102	5.63
162.8	.017	509.3	373.2	-.99	.782	-257	-11.2	-2.64	2.706	-.584	1.15	102.05	.108	5.67
Microphone angle, 120°														
242.3	0.0158	368	375	-1.42	0.748	-288	113	-2.17	2.26	-0.839	1.58	115.6	0.07	7.66
224.6	.013	396		-1.197	.647	-279	111.2	-2.2	2.46	-.839	1.48	112.3	.058	7.28
210	.014	443		-1.04	.685	-269	114.2	-2.19	2.29	.827	1.39	109.6	.0399	7.93
192.3	.0127	437		-1.19	.743	-270	66.6	-2.28	2.47	-.784	1.23	106.4	.0439	7.77
162.8	.0346	460.2	374.5	-1.15	.735	-265	33.6	-2.48	2.76	-.709	1.21	101.42	.0614	8.57
Microphone angle, 140°														
242.3	0.0274	382	375	-1.88	1.21	-288	-79.9	-2.25	2.66	-0.727	1.24	114.7	0.0102	7.2
224.6	.034	432	375	-1.56	1.028	-279	-18.6	-2.35	2.2	-.76	1.23	111	.0276	5.18
210	.039	464	328	-1.53	.896	-277	106	-2.22	2.25	-.714	1.22	110	.029	9.3
192.3	.043	383	375	-1.91	.791	-287.5	-111.2	-2.38	3.84	-.59	1.35	108.98	.130	5.12
162.8	.047	417	375	-1.76	.711	-281	-89.96	-2.45	4.08	-.529	1.31	104.47	.056	4.628

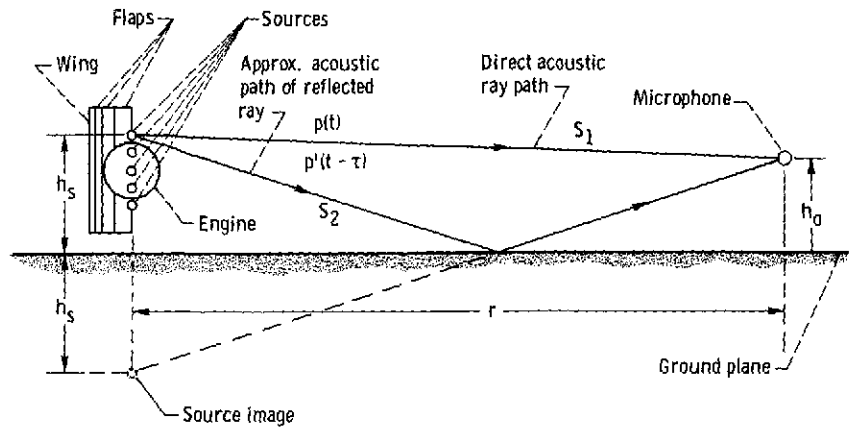

(a) Source and microphone geometry with respect to ground plane.

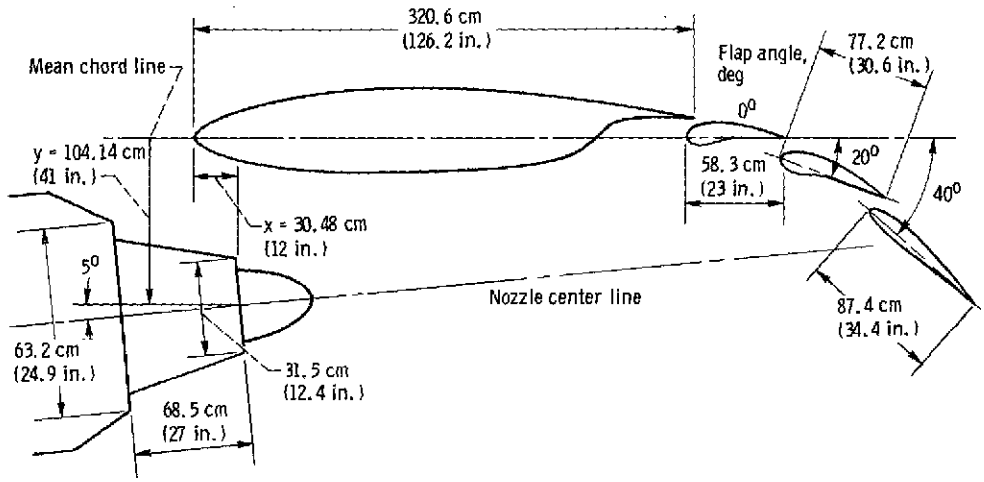

(b) Turbofan engine under-the-wing in externally blown-flap test configuration at takeoff flap setting of 0^0-20^0-40^0.

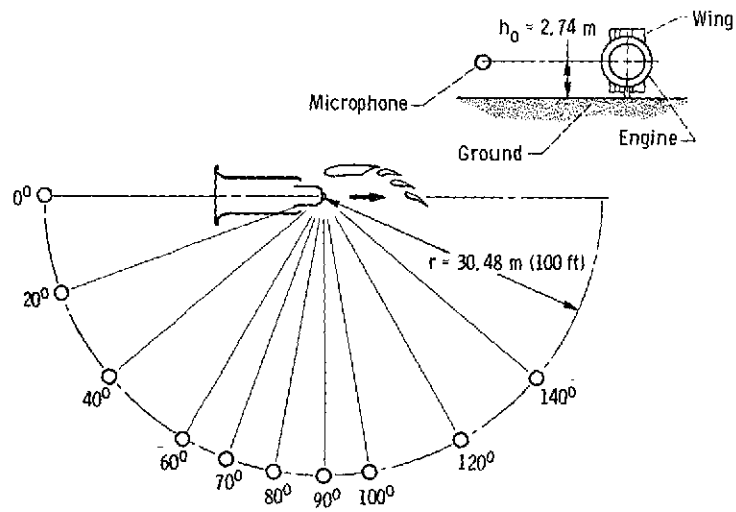

(c) Microphone array. At 100^0 measurements also taken at $1/2\ h_0$ and $2h_0$.

Figure 1. - Test facility geometry (ref. 2).

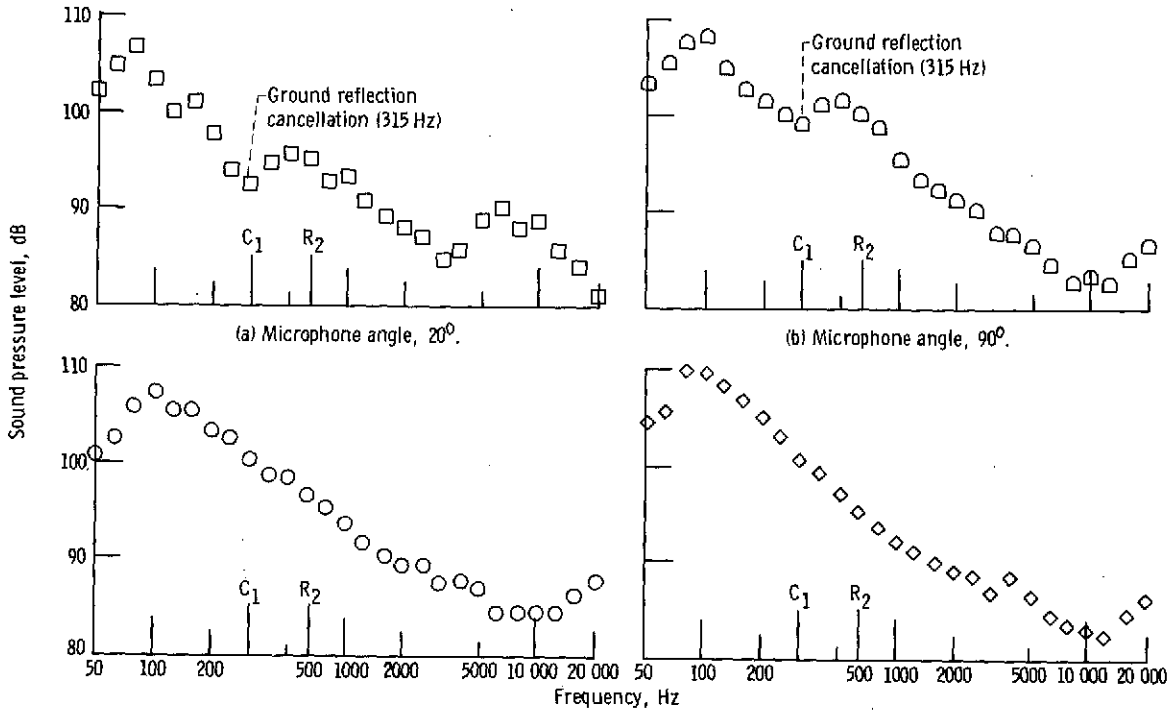

Figure 2. - Typical one-third-octave sound power level spectra from under-the-wing, turbofan engine, externally blown-flap test configuration (ref. 1). Effective exhaust velocity, 242.3 meters per second (795 ft/sec); distance from source, 30.48 meters (100 ft); microphone height, 2.7 meters (9 ft).

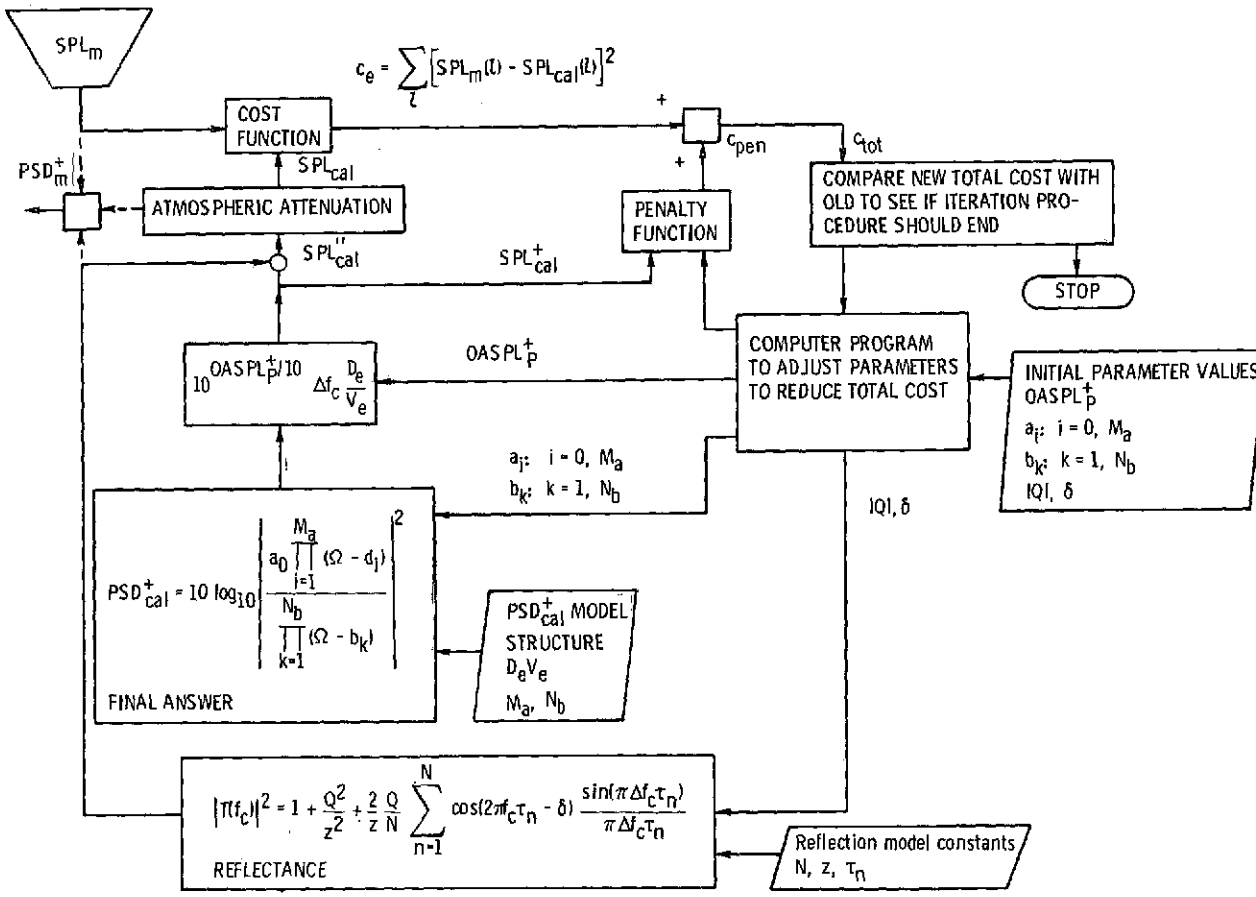

Figure 3. – Diagram of computer method.

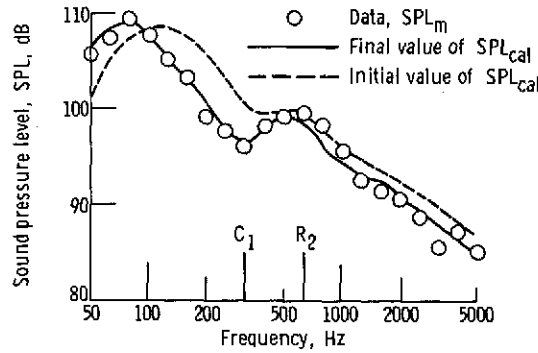

(a) Comparison of calculated and measured sound pressure level.

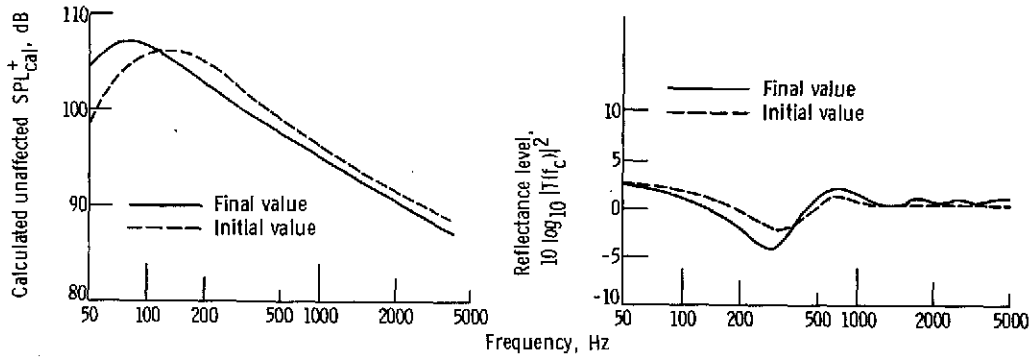

(b) Calculated unaffected sound pressure level.

(c) Calculated reflectance level.

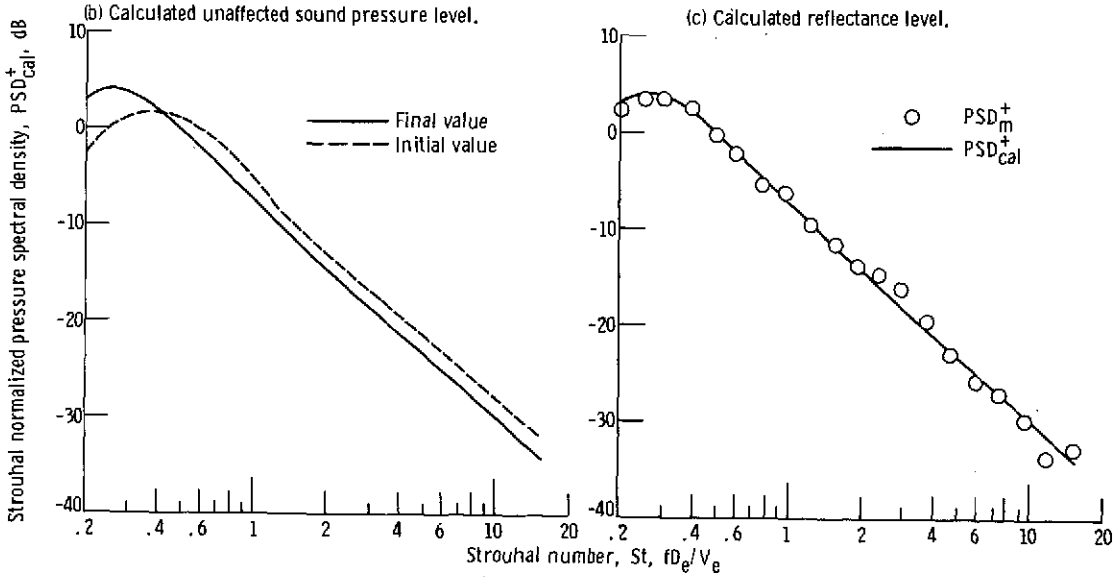

(d) Calculated Strouhal normalized pressure spectral density.

(e) Comparison of PSD^+ based on measured data corrected with the hypothetical reflection effect (PSD^+_m) and PSD^+ as calculated from curve fit (PSD^+_{cal}).

Figure 4. - Initial and final iteration values of SPL, SPL^+, $|T(f_c)|^2$ and PSD^+_{cal}. Microphone 60° from inlet. Effective exhaust velocity, 242.3 meters per second (795 ft/sec); distance, 30.48 meters (100 ft); microphone height, 2.74 meters (9 ft); engine centerline height, 2.74 meters (9 ft).

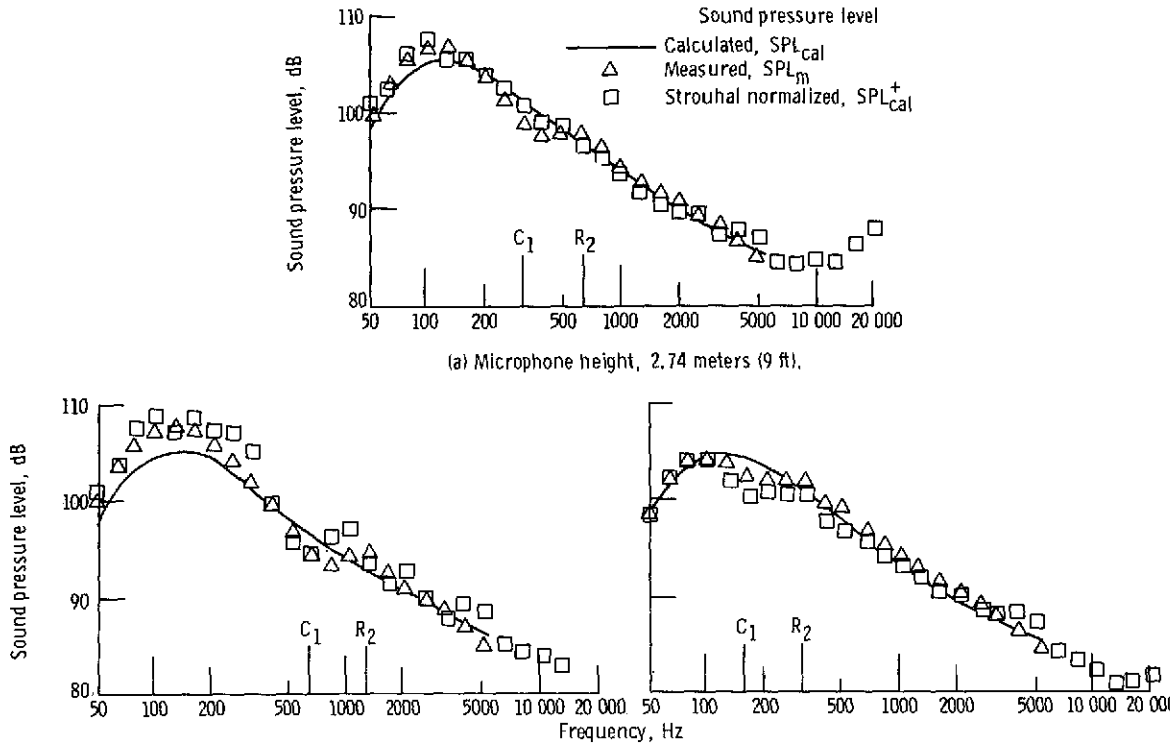

(a) Microphone height, 2.74 meters (9 ft).

(b) Microphone height, 1.37 meters (4.5 ft).

(c) Microphone height, 5.49 meters (18 ft).

Figure 5. - Comparison of SPL_{cal}, SPL_m and SPL^+_{cal} one-third-octave spectra at three microphone heights. Microphone angle, 100^0. Effective exhaust velocity, 242.3 meters per second (795 ft/sec); distance, 30.48 meters (100 ft).

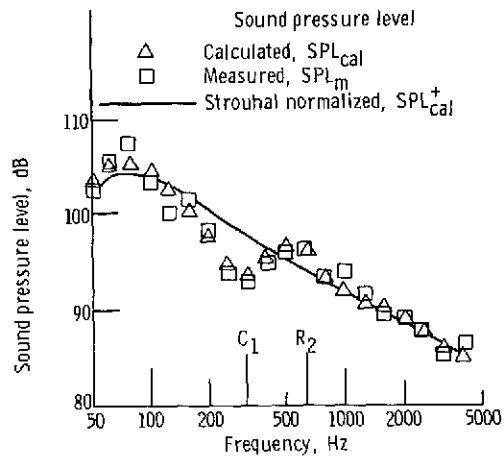

Figure 6. - Comparison of SPL_{cal}, SPL_m, and SPL^+_{cal} for largest magnitude of reflected-ray impedance (Q = 0.5) evaluated by computer procedure. Microphone angle, 20^0; effective exhaust velocity, 242.3 meters per second (795 ft/sec); microphone distance, 30.48 meters (100 ft); microphone height, 2.74 meters (9 ft).

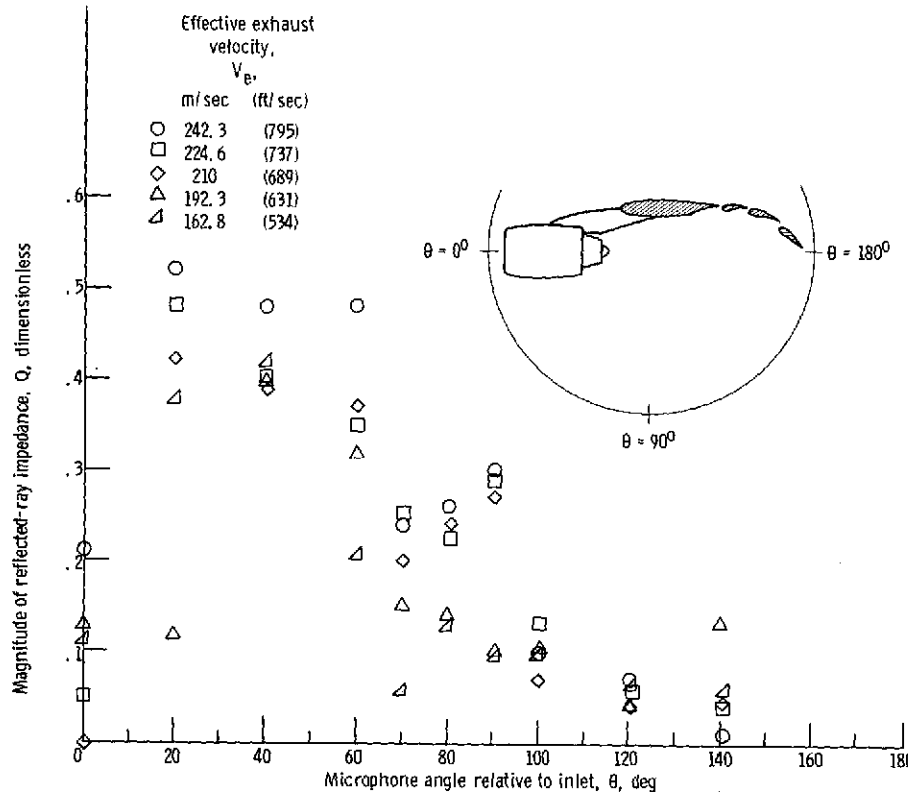

Figure 7. - Variation of magnitude of reflected-ray transfer function with angle for a range of velocities.

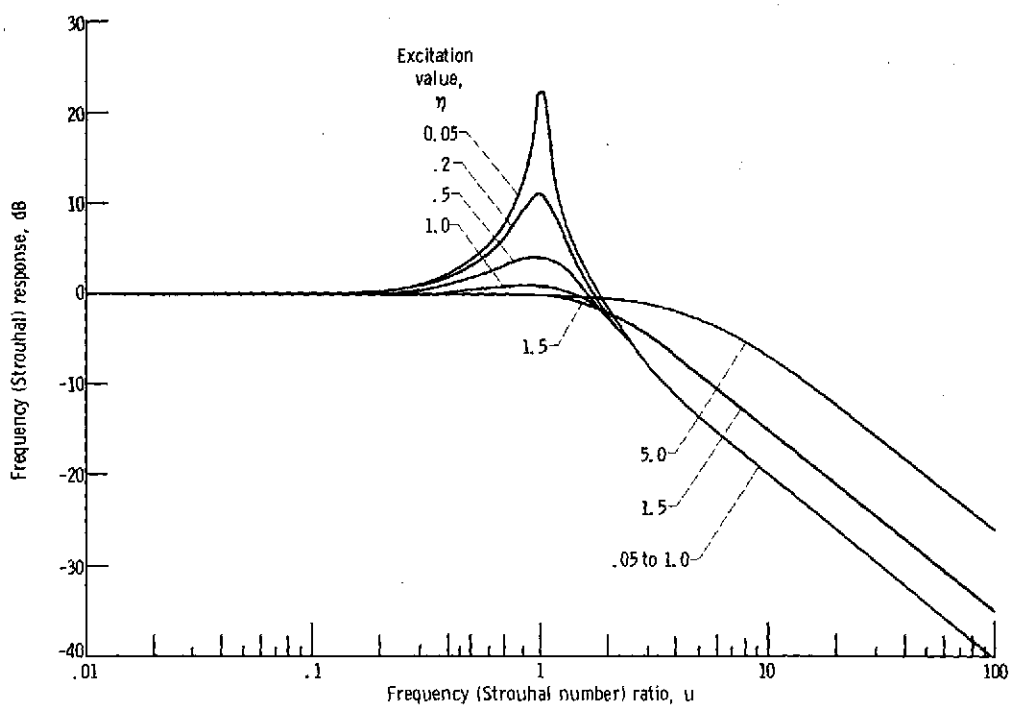

Figure 8. - Basic frequency (Strouhal) response function (-E(u, ηc)) for various frequency (Strouhal) response excitation values.

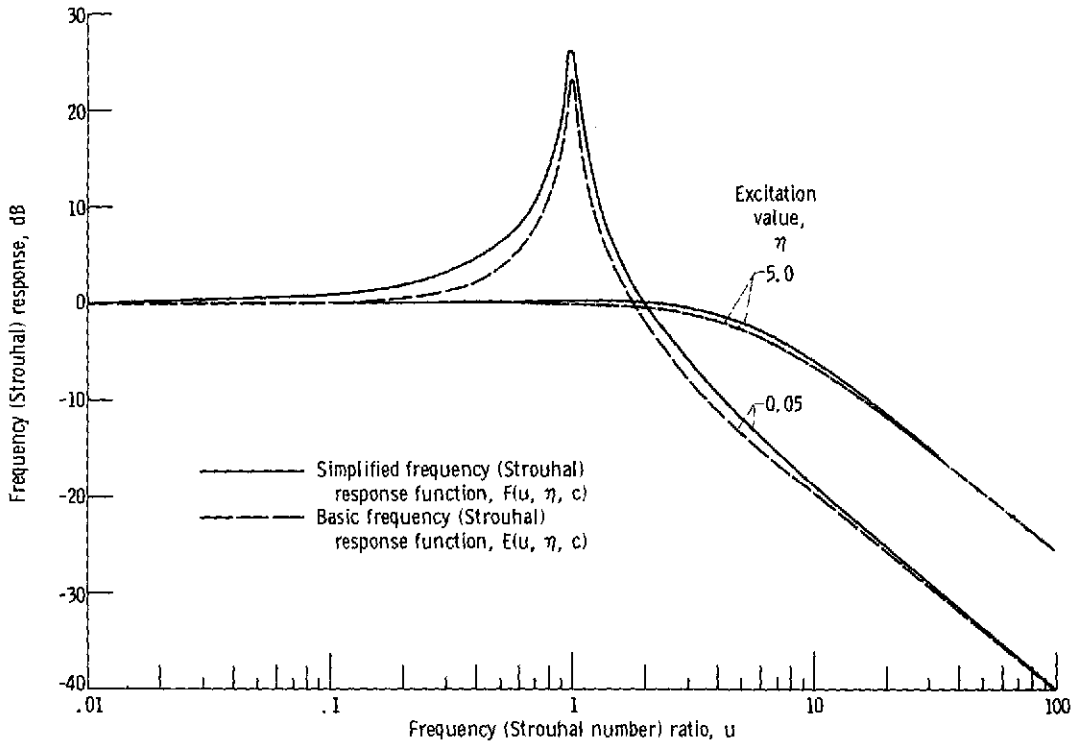

Figure 9. - Comparison of basic and simplified frequency (Strouhal) response function at frequency (Strouhal) response excitation (η) value of 0.05 and 5.0.

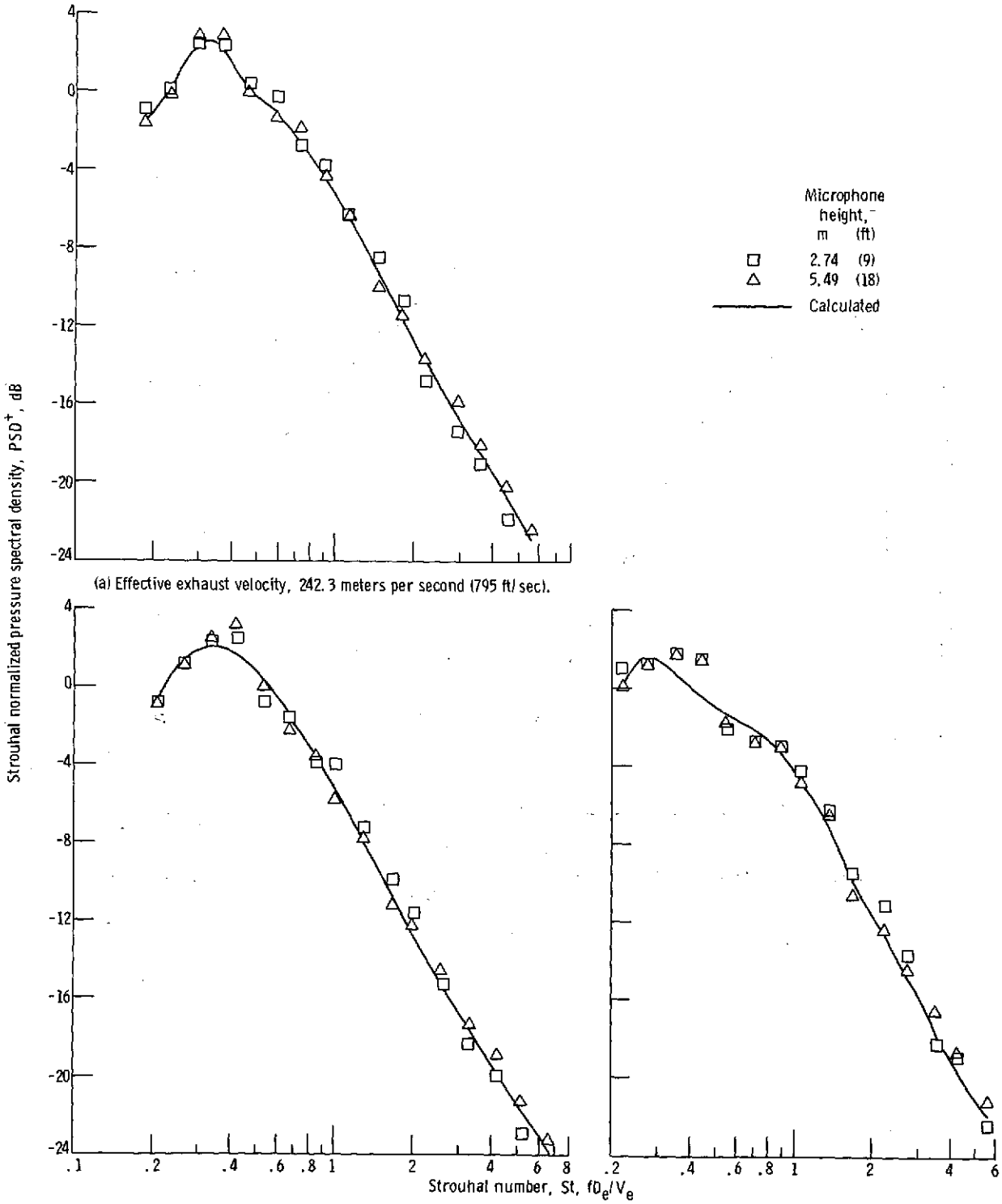

(a) Effective exhaust velocity, 242.3 meters per second (795 ft/sec).

(b) Effective exhaust velocity, 224.6 meters per second (737 ft/sec).

(c) Effective exhaust velocity, 210.0 meters per second (689 ft/sec).

Figure 10. - Comparison of calculated with measured PSD^+ for different effective exhaust velocities. Microphone angle, 100°.

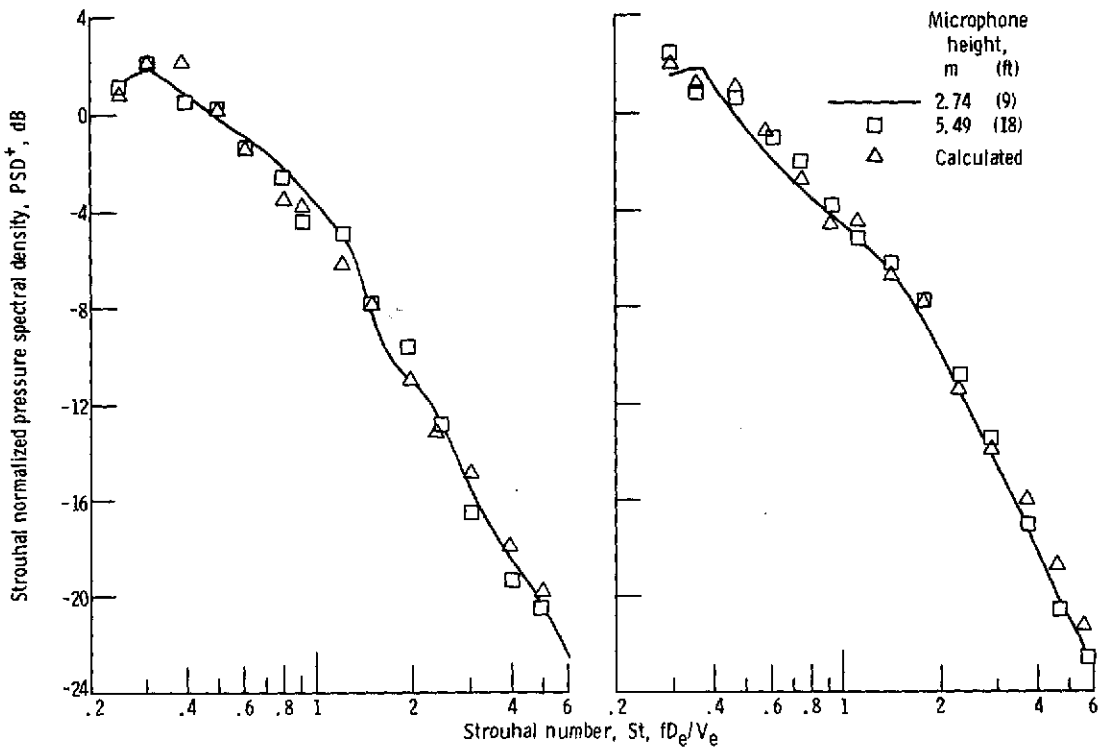

(d) Effective exhaust velocity, 192.3 meters per second (631 ft/sec).

(e) Effective exhaust velocity, 162.8 meters per second (534 ft/sec).

Figure 10. - Concluded.

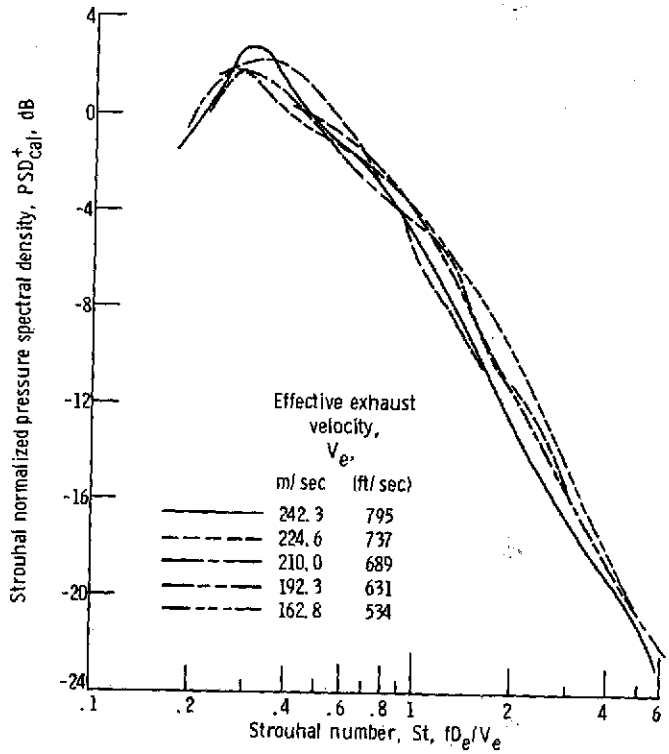

Figure 11. - Effect of velocity on calculated PSD^{+}_{cal} for microphone at 100^0

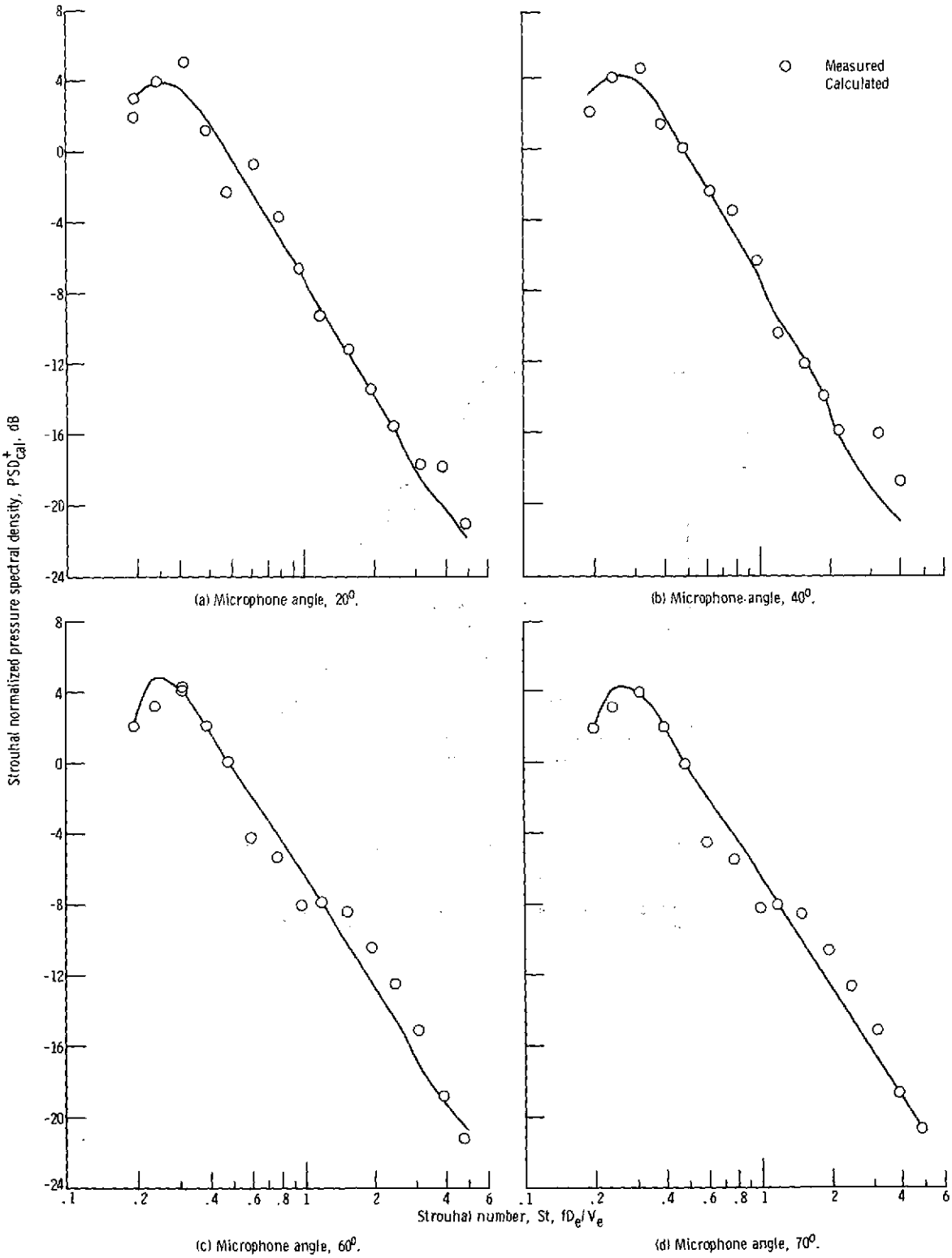

Figure 12. - Comparison of calculated and measured PSD^{+} at various angles. Effective exhaust velocity, 242.3 meters per second (795 ft/sec).

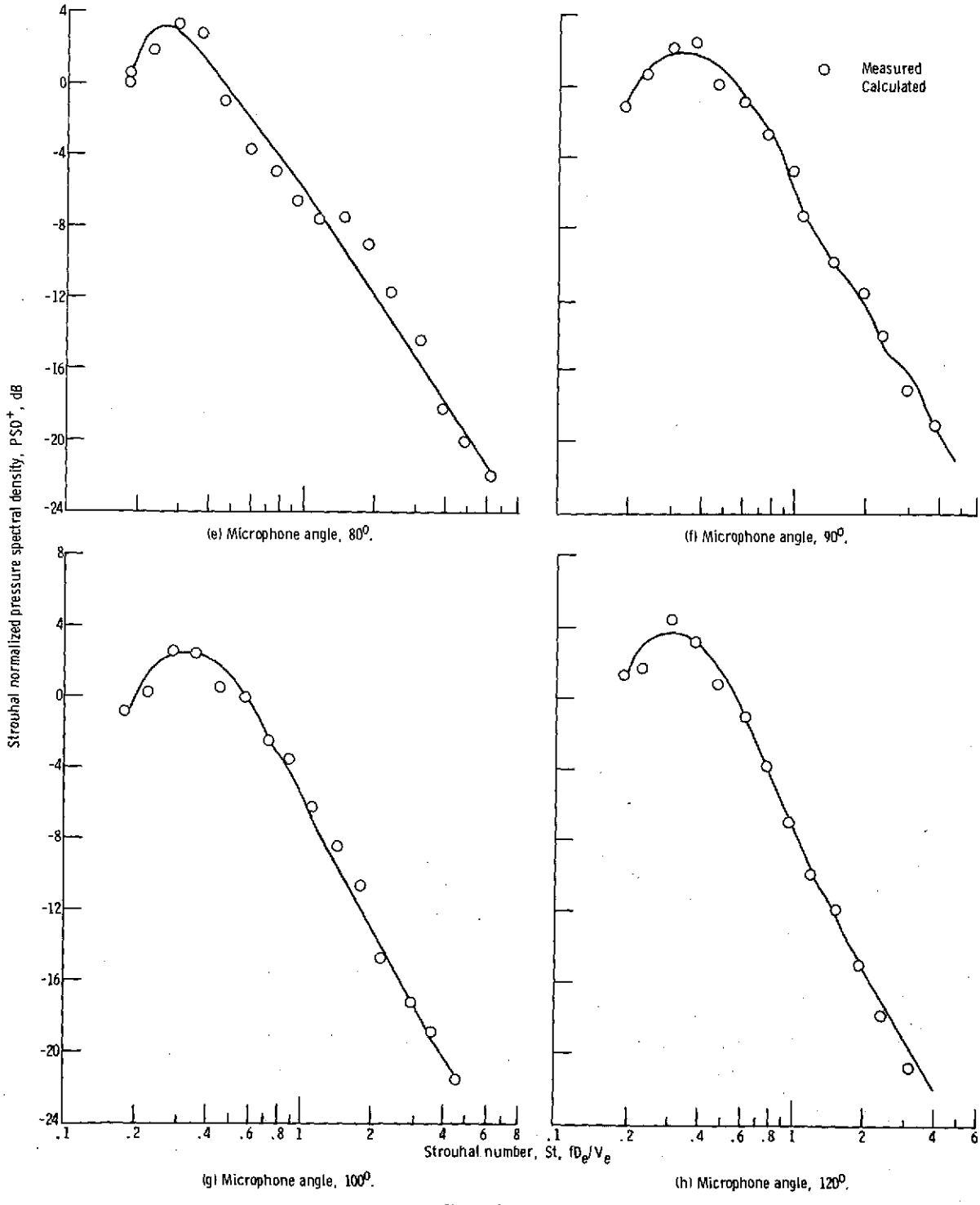

Figure 12. - Concluded.

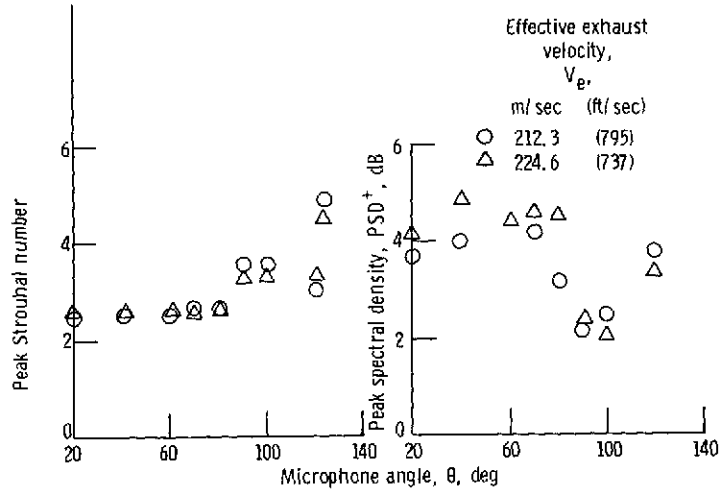

(a) Variation of peak Strouhal number.

(b) Variation of peak value.

Figure 13. - Variation of peak Strouhal number and peak value of calculated PSD^{+} with microphone angle.

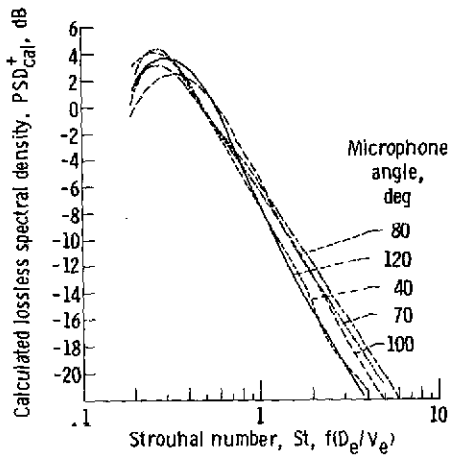

Figure 14. - Variation of calculated lossless spectral density. Effective exhaust velocity, 242.3 meters per second (795 ft/sec); turbofan engine externally blown-flap configuration; flap setting, 0^{0}-20^{0}-40^{0}.

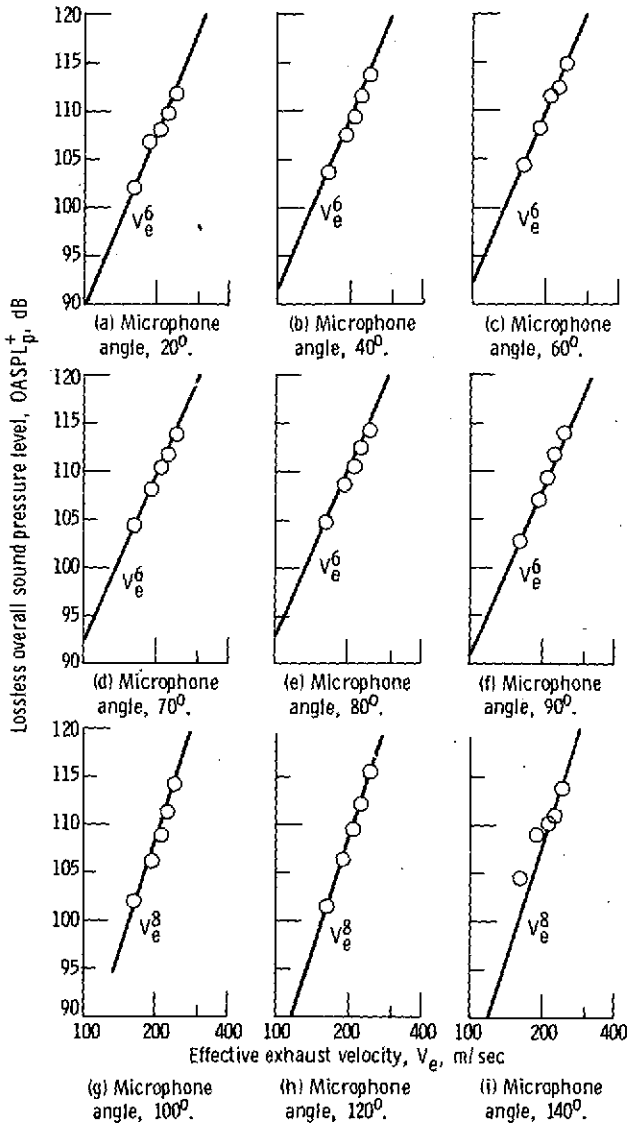

Figure 15. - Variation of lossless overall sound pressure level with effective velocity. Turbofan engine externally blown-flap configuration; flap setting, 0^0-20^0-40^0; microphone radius, 30.48 meters (100 ft).